JAERI-Tech
95-056

PREIRRADIATION CHARACTERIZATION OF HTGR FUEL FOR HRB-22 CAPSULE IRRADIATION TEST (JAERI/USDOE COLLABORATIVE IRRADIATION TEST FOR HTGR FUEL)

January 1996

Kazuo MINATO, Hironobu KIKUCHI, Kazuhiro SAWA
Tsutomu TOBITA and Kousaku FUKUDA

日本原子力研究所
Japan Atomic Energy Research Institute

本レポートは，日本原子力研究所が不定期に公刊している研究報告書です。
入手の問合わせは，日本原子力研究所技術情報部情報資料課(〒319-11 茨城県那珂郡東海村）あて，お申し越しください。なお，このほかに財団法人原子力弘済会資料センター（〒319-11 茨城県那珂郡東海村日本原子力研究所内）で複写による実費頒布をおこなっております。

This report is issued irregularly.
Inquiries about availability of the reports should be addressed to Information Division, Department of Technical Information, Japan Atomic Energy Research Institute, Tokai-mura, Naka-gun, Ibaraki-ken 319-11, Japan.

編集兼発行　日本原子力研究所
印　　刷　㈱高野高速印刷

Preirradiation Characterization of HTGR Fuel for HRB-22 Capsule Irradiation Test (JAERI/USDOE Collaborative Irradiation Test for HTGR Fuel)

Kazuo MINATO, Hironobu KIKUCHI, Kazuhiro SAWA
Tsutomu TOBITA and Kousaku FUKUDA

Department of Chemistry and Fuel Research
Tokai Research Establishment
Japan Atomic Energy Research Institute
Tokai-mura, Naka-gun, Ibaraki-ken

(Received December 8, 1995)

As a JAERI/USDOE collaborative irradiation test for high-temperature gas-cooled reactors fuel, a capsule irradiation test of JAERI fuel compacts in the High Flux Isotope Reactor followed by postirradiation examinations at the Oak Ridge National Laboratory was planed. This report describes fabrication processes and preirradiation characterization of the JAERI fuels for the HRB-22 capsule irradiation test. The fuel compact contained Triso-coated fuel particles and dummy particles which were needed to adjust a linear heat rate of the fuel. The preirradiation characterization was performed of the Triso-coated fuel particles, the dummy particles and the fuel compacts. Impurities, dimensions, densities, free uranium fractions, SiC-defective fractions, etc. were measured. The fuels were observed by optical microscopy, X-ray microradiography and scanning electron microscopy. The preirradiation characterization revealed that the fuels were suitable for the irradiation test and of good quality.

Keywords : Coated Fuel Particles, HTGR, Fuel Kernel, Silicon Carbide, Pyrolytic Carbon, Fabrication, Characterization, Irradiation

ＨＲＢ－22キャプセル照射試験用高温ガス炉燃料の照射前特性評価
（日米高温ガス炉燃料共同照射試験）

日本原子力研究所東海研究所燃料研究部
湊　　和生・菊地　啓修・沢　　和弘・飛田　　勉・福田　幸朔

（1995年12月８日受理）

高温ガス炉燃料の日米共同照射試験として，原研で開発を進めている燃料コンパクトを米国オークリッジ国立研究所のＨＦＩＲで照射し，引き続き照射後試験を同所で実施することが計画された。本報告書は，日米共同ＨＲＢ－22キャプセル照射試験用の原研燃料の製造プロセス及び照射前特性評価試験について記述したものである。この照射試験用の燃料コンパクトには，被覆燃料粒子のほかに，発熱量の調整のために模擬粒子が含まれていた。照射前特性評価試験は，被覆燃料粒子，模擬粒子及び燃料コンパクトを対象とし，不純物，寸法，密度，露出ウラン率，ＳｉＣ層破損率などを測定した。また，光学顕微鏡，Ｘ線ラジオグラフィ及び走査電子顕微鏡により，燃料を観察した。その結果，これらの燃料コンパクトは，照射試料として適していること及び高い品質であることが明らかになった。

東海研究所：〒319－11　茨城県那珂郡東海村白方白根２－４

Contents

目　　次

1. INTRODUCTION

Within an international collaborative program between the Japan Atomic Energy Research Institute (JAERI) and the U. S. Department of Energy (USDOE) on cooperation in research and development in the area of High-Temperature Gas-Cooled Reactors (HTGR), an irradiation test of JAERI fuel compacts was planned. The fuels were loaded in HRB-22 capsule and irradiated in the High Flux Isotope Reactor (HFIR) at the Oak Ridge National Laboratory (ORNL).

The fuels for the HRB-22 capsule irradiation test, which were fabricated by the Nuclear Fuel Industries, Ltd. (NFI), are Triso-coated fuel particles dispersed in graphite matrix to form fuel compacts. The Triso-coated fuel particle consists of a microspherical kernel of uranium dioxide (UO_2) fuel and coating layers of porous pyrolytic carbon (PyC), inner dense PyC (IPyC), silicon carbide (SiC) and outer dense PyC (OPyC). In the fuel compacts for the HRB-22 capsule irradiation test, SiC-kerneled coated particles, dummy particles, were contained to attain a target irradiation temperature of around 1300°C, keeping the packing fraction of the particles in a fuel compact unchanged. The dummy particles were needed because of an accelerated irradiation of the HRB-22 test.

The fuel design for the HRB-22 capsule irradiation test is called the advanced fuel, which is different from that for the initial core fuels of the High Temperature Engineering Test Reactor (HTTR) being built at the Oarai Research Establishment of JAERI [1]. A target burnup of the advanced fuel is 10 %FIMA, whereas that of the HTTR fuel is 3.6 %FIMA. In the advanced fuel design, the diameter of the fuel kernel is smaller and the porous PyC layer, called the buffer layer, and the SiC layer are thicker than those of the HTTR fuel.

For the collaboration, twenty fuel compacts were sent to ORNL from JAERI. Twelve out of twenty fuel compacts were encapsulated and irradiated in HFIR. The rest of the fuel compacts were used for preparatory examinations in a hot cell or are stored at ORNL. At JAERI ten fuel compacts are stored, some of which were used for the preirradiation characterization.

This report describes the fabrication processes and preirradiation characterization of the coated fuel particles, the dummy particles and the fuel compacts for the HRB-22 capsule irradiation test.

2. FABRICATION PROCESSES OF FUELS

2.1 Fabrication Process of Coated Fuel Particles

The fabrication process of UO_2 kernels was the gel-precipitation method [1,2]. Uranyl nitrate ($UO_2(NO_3)_2$) solution mixed with additives which controls the viscosity of the solution was dropped through vibrating nozzles into ammonia solution (NH_4OH) to form ammonium diuranate (ADU) spheres. After washing with water and alcohol and drying, the ADU spheres were calcinated to produce UO_3 spheres. The UO_2 kernels were obtained by sintering the UO_3 spheres. Figure 2.1 shows the fabrication process of the UO_2 kernels.

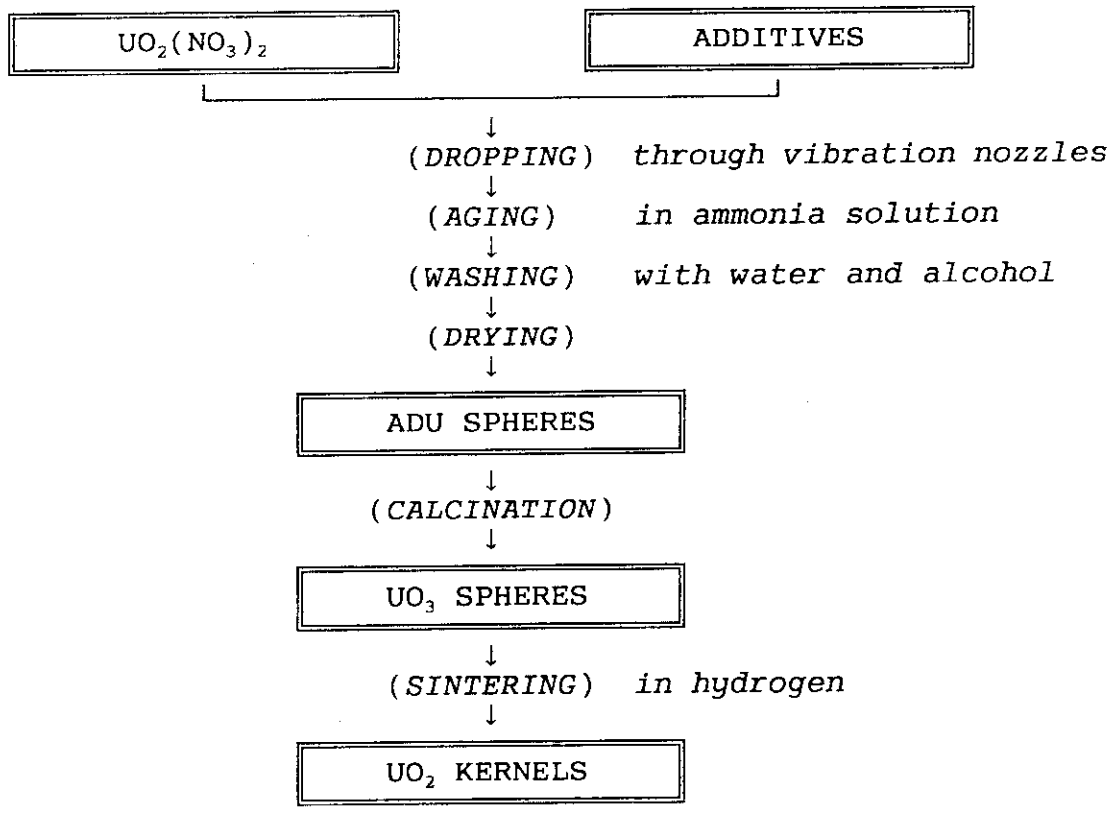

Fig. 2.1 Fabrication process of UO_2 kernels.

The coating of the UO_2 kernels was performed in a fluidized bed coater [1,2]. The buffer layer of porous pyrolytic carbon was deposited on the UO_2 kernels by the pyrolysis of acetylene (C_2H_2) in the presence of argon (Ar), and the IPyC and the OPyC layers of dense

pyrolytic carbon were deposited by the pyrolysis of propylene (C_3H_6) in the presence of argon. The SiC layer was chemically vapor deposited using methyltrichlorosilane (CH_3SiCl_3, MTS) and hydrogen (H_2). Figure 2.2 summarizes the coating process of the UO_2 kernels.

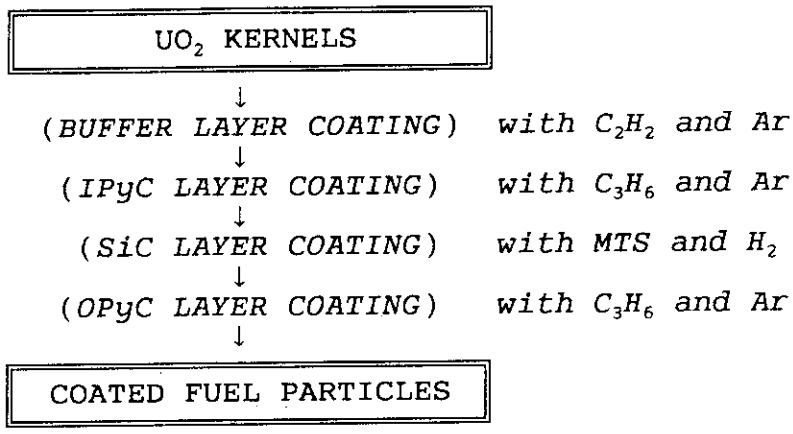

Fig. 2.2 Coating process of UO_2 kernels.

2.2 *Fabrication Process of Dummy Particles*

The dummy particles were prepared by coating the SiC kernels in the fluidized bed coater. The SiC kernels were produced by powder metallurgy. The SiC kernels were coated by the IPyC layer of dense pyrolytic carbon, the SiC layer and the OPyC layer in the same manner as in the fabrication of the coated fuel particles, as shown in Fig. 2.3. No buffer layer was present in the dummy particles.

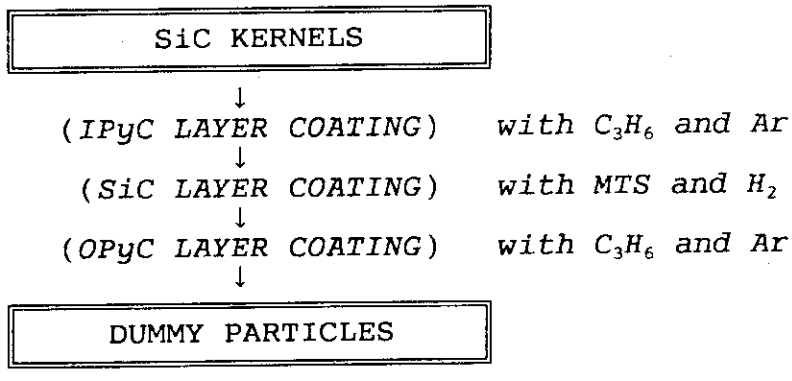

Fig. 2.3 Coating process of dummy particles.

2.3 *Fabrication Process of Fuel Compacts*

The fabrication process of the fuel compacts was the overcoat/press method [1,2], which is shown in Fig. 2.4. The coated fuel particles and the dummy particles were overcoated by the resinated graphite powder with alcohol. The resinated graphite powder was prepared by mixing electrographite powder, natural graphite powder and phenol resin as a binder in the ratio 16:64:20, followed by grinding the mixture to powder. The overcoated fuel and dummy particles were warm-pressed by dies to form annular-shaped green fuel compacts. The green fuel compacts were heat-treated at 800°C in N_2 to carbonize the binder and at 1800°C in vacuum to degas the fuel compacts.

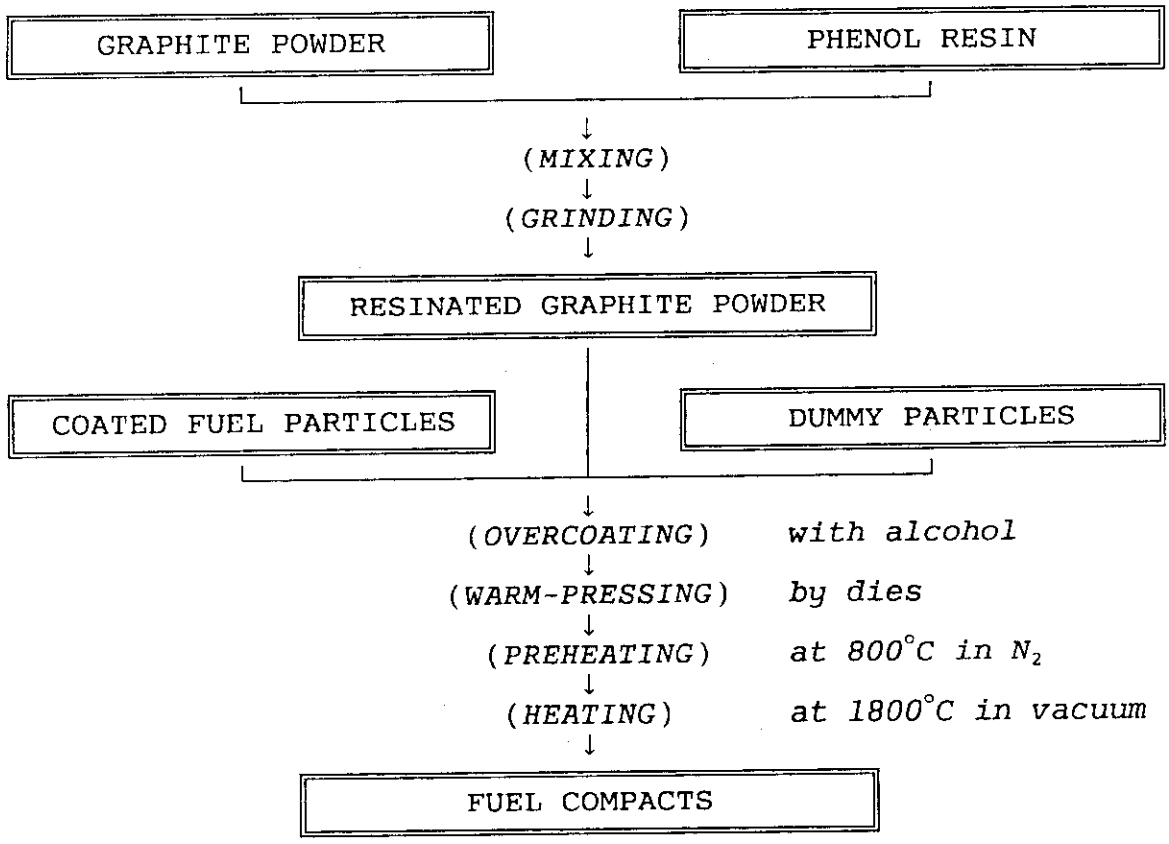

Fig. 2.4 Fabrication process of fuel compacts.

3. CHARACTERIZATION OF FUELS

3.1 Characterization of Coated Fuel Particles

3.1.1 Enrichment of U-235

The enrichment of U-235 of the starting U_3O_8 powder was 4.07 mass% determined by γ-ray spectrometry.

3.1.2 O/U ratio of fuel kernels

The O/U ratio of the UO_2 kernels was 2.00 measured by gravimetric method.

3.1.3 Impurities in fuel kernels

The contents of 25 elements were analyzed in the UO_2 kernels. The results are summarized in Table 3.1.

Table 3.1 Impurities in fuel kernels

Element	Content (ppm)	Method
Ag	< 0.6	Emission spectrochemical analysis
Al	<10	Emission spectrochemical analysis
B	< 0.4	Emission spectrochemical analysis
C	<10	Induction heating coulometry
Ca	44	Emission spectrochemical analysis
Cd	< 0.1	Emission spectrochemical analysis
Cl	<10	Pyrohydrolysis spectrophotometry
Cr	< 5	Emission spectrochemical analysis
Cs	< 0.002	Activation analysis
Cu	< 4	Emission spectrochemical analysis
Dy	< 0.05	Emission spectrochemical analysis
Eu	< 0.05	Emission spectrochemical analysis
F	< 1	Pyrohydrolysis spectrophotometry
Fe	<20	Emission spectrochemical analysis

Gd	< 0.05	Emission spectrochemical analysis
Mg	< 4	Emission spectrochemical analysis
Mo	< 5	Emission spectrochemical analysis
N	<10	Molecular absorption spectrophotometry
Ni	<12	Emission spectrochemical analysis
Pb	< 6	Emission spectrochemical analysis
Pd	< 0.02	Activation analysis
Ru	< 5	Activation analysis
Si	8	Emission spectrochemical analysis
Sm	< 0.05	Emission spectrochemical analysis
Sn	< 3	Emission spectrochemical analysis

3.1.4 Dimensions of coated fuel particles

The diameter of the UO_2 kernels was measured on 1083 kernels by the Particle Size Analyzer (PSA) [3]. The thicknesses of the buffer and the IPyC layers were measured on 200 particles polished to the equator by optical microscopy. The thicknesses of the SiC and the OPyC layers were measured on 200 particles by X-ray microradiography. The diameter of the coated fuel particles was measured on 1058 particles by PSA. The results are summarized in Table 3.2. All the measured values for the coating thicknesses on 200 particles are listed in Appendix A.

Table 3.2 Dimensions of coated fuel particles

	Mean (μm)	Standard deviation (μm)
Kernel diameter	544	9.1
Buffer thickness	97.4	12.9
IPyC thickness	32.9	3.4
SiC thickness	33.7	1.6
OPyC thickness	39.3	3.1
Particle diameter	950	26.6

3.1.5 *Density of coated fuel particles*

The densities of the UO_2 kernel and the buffer layer were measured by mercury pycnometry on two samples of 4 g-kernels and on two samples of 4 g-buffer-coated particles. The density of the IPyC layer was measured on ten fragments of the layer by the sink-float method using tetrabromoethane ($CHBr_2CHBr_2$) and ethanol (CH_3CH_2OH). The sink-float method was applied to the measurement of the SiC density on ten fragments using tetrabromoethane and methylene iodide (CH_2I_2). The density of the OPyC layer was measured on two samples of 4 g-coated particles by n-butanol pycnometry. The density of the coated fuel particle was measured by two methods: on 1058 coated particles by PSA and on two 4 g-coated particles by n-butanol pycnometry. The results are listed in Table 3.3.

Table 3.3 Density of coated fuel particles

	Mean (Mg/m^3)	Method
Kernel density	10.84	Mercury pycnometry
Buffer density	1.10	Mercury pycnometry
IPyC density	1.85	Sink-float method
SiC density	3.20	Sink-float method
OPyC density	1.85	n-butanol pycnometry
Particle density	3.78	PSA
	3.67	n-butanol pycnometry

3.1.6 *OPTAF and crystallite size of PyC layers*

The optical anisotropy factors (OPTAF) of the IPyC and the OPyC layers were measured on five particle-cross sections. On each cross section four points were sampled. The measured value was 1.00 for both the IPyC and the OPyC layers. The crystallite size of L_c of the OPyC layer was found to be 230 nm by X-ray diffractometry.

3.1.7 *Sphericity of kernels and coated fuel particles*

The sphericity is defined as the ratio of maximum diameter to minimum diameter (d_{max}/d_{min}) of a particle. PSA was used to measure the sphericity on 100 kernels and 100

coated fuel particles. All kernels measured were $d_{max}/d_{min} \leq 1.2$. For the coated fuel particles, 97 out of 100 particles were $d_{max}/d_{min} \leq 1.2$.

3.1.8 Crushing strength of coated fuel particles

The crushing strength of the coated fuel particles was measured on 50 particles by uni-axial compression test. The data was analyzed with the Weibull statistic theory as shown in Fig. 3.1. The 50%-failure strength (median strength) was 23.0 N and the Weibull parameter was 7.5. All the measured data is listed in Appendix B.

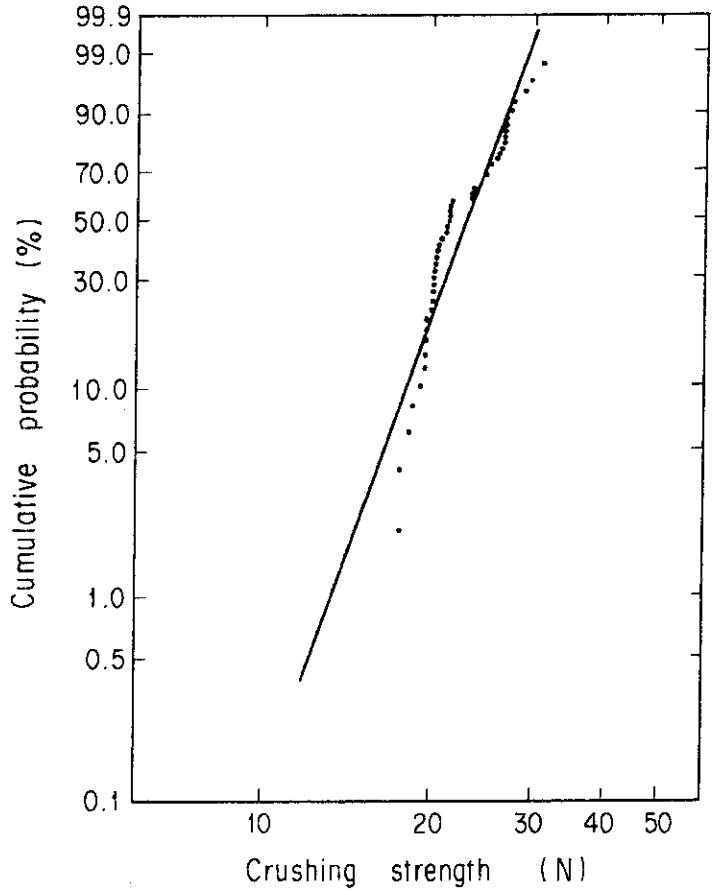

Fig. 3.1 Crushing strength of the Triso-coated fuel particles.

3.1.9 Free uranium fraction of coated fuel particles

The free uranium fraction of the coated fuel particles was measured by the acid leaching. Five samples of 30 g-particles were boiled in 7 mol/l nitric acid (HNO_3) for 20 h, and the solution was analyzed for uranium by both fluorometric and colorimetric analyses. The measured values, as shown in Table 3.4, mean that no through-coating failure was present in the samples, for 30 g-particles correspond to about 18000 particles.

Table 3.4 Free uranium fraction of coated fuel particles

	Fluorometric	Colorimetric
Sample A1	1.9×10^{-7}	3.3×10^{-7}
Sample A2	2.9×10^{-7}	3.3×10^{-7}
Sample A3	3.0×10^{-7}	5.6×10^{-7}
Sample A4	2.3×10^{-7}	3.3×10^{-7}
Sample A5	2.2×10^{-7}	5.3×10^{-7}

3.1.10 SiC-defective fraction of coated fuel particles

The SiC-defective fraction of the coated fuel particles was measured by the burn/leach method. Five samples of 20 g-particles were burned at 900°C in the air and the heating was continued for 6 h after the OPyC layers were burned off. The burnt samples were boiled in 7 mol/l nitric acid for 5 h and the solution was analyzed for uranium by both fluorometric and colorimetric analyses. The measured values shown in Table 3.5 mean that no SiC-defective particle was present in the samples, for 20 g-particles correspond to about 12000 particles.

Table 3.5 SiC-defective fraction of coated fuel particles

	Fluorometric	Colorimetric
Sample B1	3.2×10^{-7}	3.3×10^{-7}
Sample B2	2.5×10^{-7}	3.3×10^{-7}
Sample B3	5.3×10^{-7}	3.6×10^{-7}
Sample B4	2.5×10^{-7}	3.3×10^{-7}
Sample B5	2.2×10^{-7}	3.3×10^{-7}

3.1.11 External view of coated fuel particles

As-fabricated UO_2 kernels, SiC-coated particles and Triso-coated fuel particles were observed by optical microscope. Typical examples are shown in Fig. 3.2.

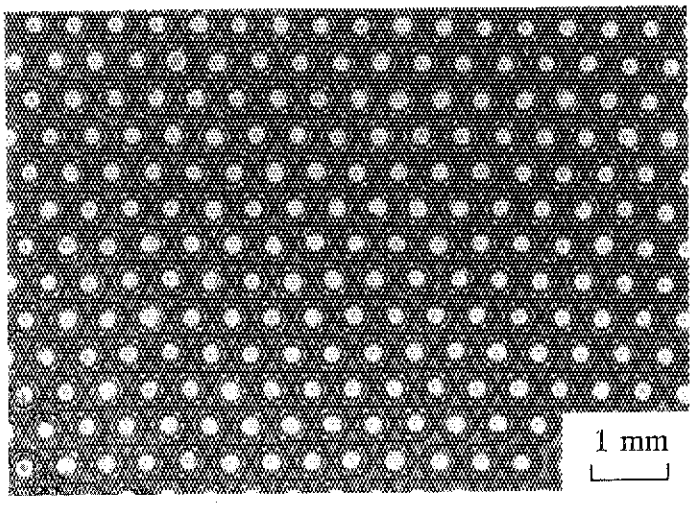

(a) UO_2 fuel kernels

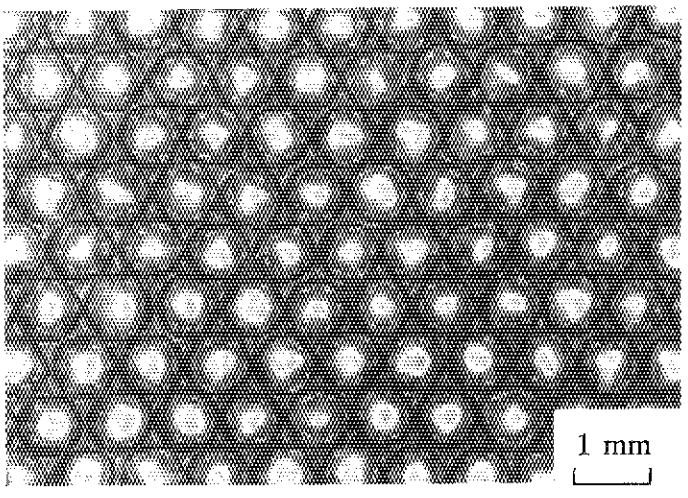

(b) SiC-coated fuel particles

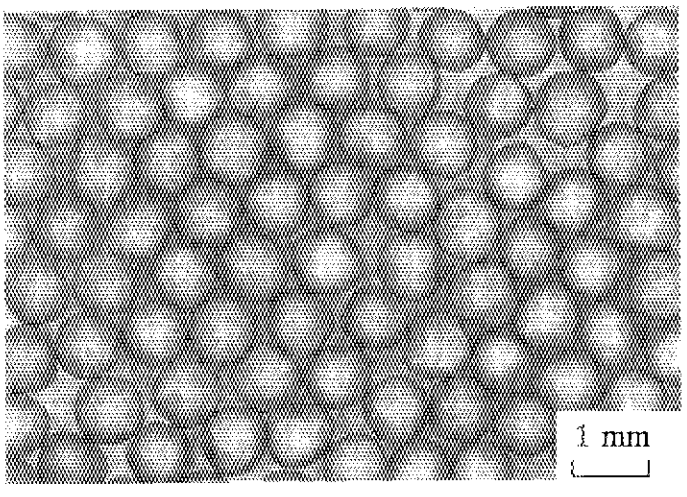

(c) Triso-coated fuel particles

Fig. 3.2 External view of as-fabricated coated fuel particles.

3.1.12 X-ray microradiography of coated fuel particles

A failure detection method of methylene iodide infusion followed by X-ray microradiography [4-6] was applied to the IPyC-coated and the Triso-coated fuel particles. By this method, through-coating failure and defects of the PyC layer can be detected. No anomaly was found by this method, as shown in Fig. 3.3.

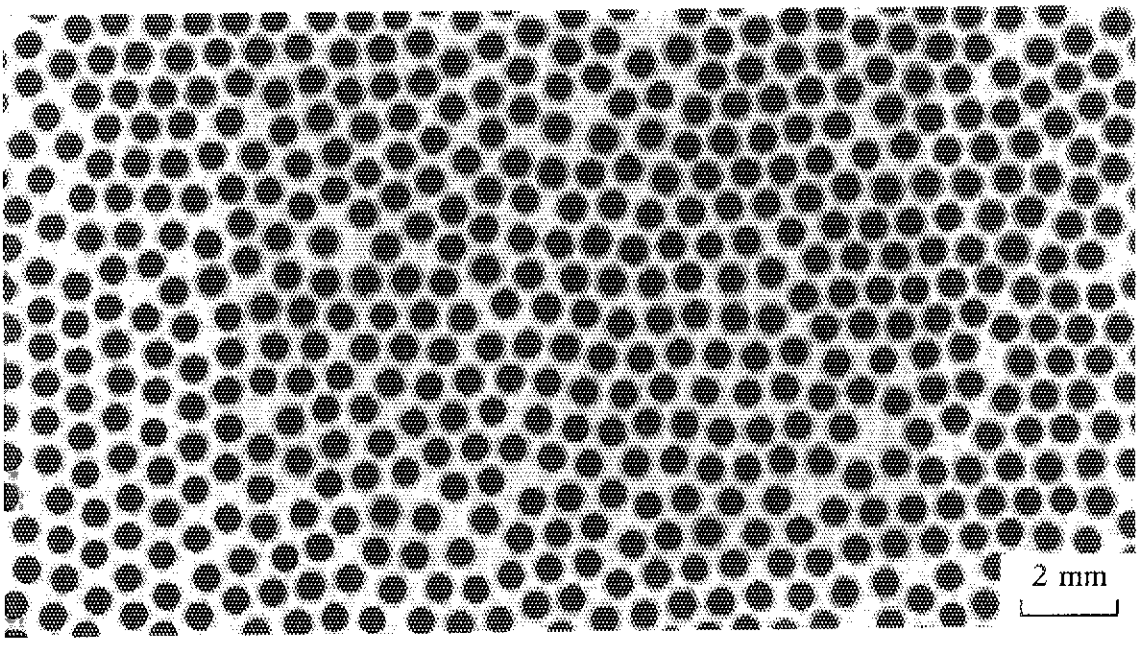

(a) IPyC-coated fuel particles

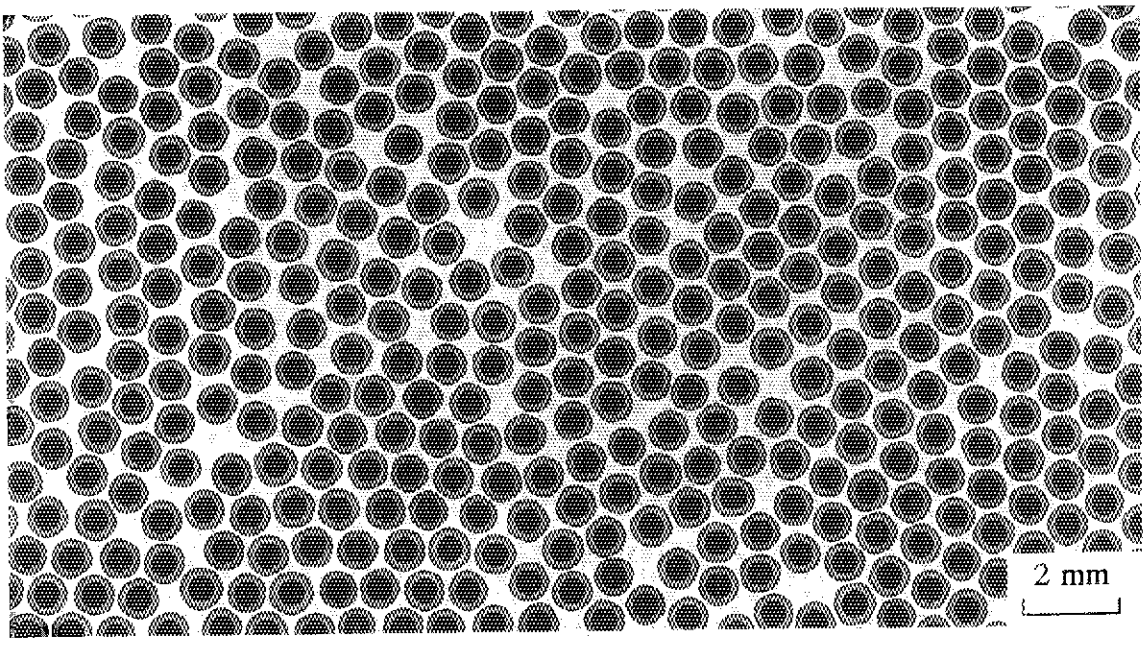

(b) Triso-coated fuel particles

Fig. 3.3 Typical examples of methylene iodide infusion/X-ray microradiographs.

3.1.13 Ceramography of coated fuel particles

Fifty Triso-coated fuel particles were embedded and polished to their equators to observe the cross section of the particles by optical microscope. The UO_2 kernels were chemically etched by a mixed solution of sulfuric acid (H_2SO_4) and hydrogen peroxide (H_2O_2) before the observation. No anomaly was found. Typical examples are shown in Fig. 3.4.

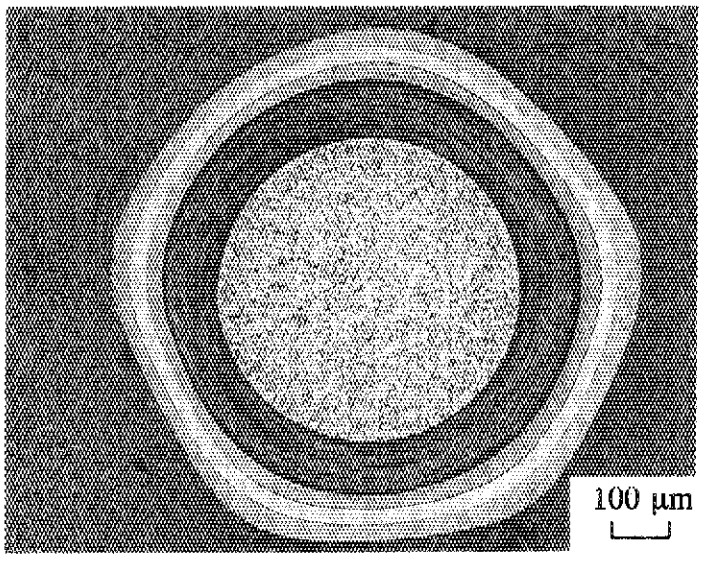

(a) The whole particle

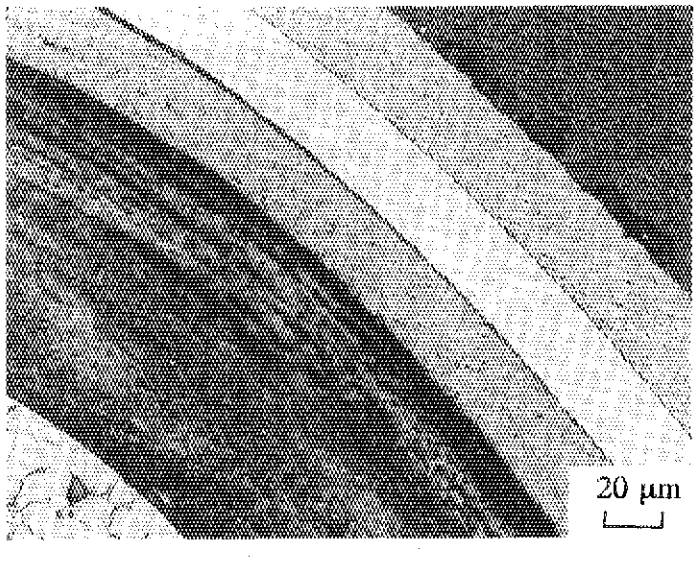

(b) Coating layers

Fig. 3.4 Typical polished cross section of the Triso-coated fuel particle.

3.1.14 Internal flaws or gold spots of SiC layers

The gold spots are caused by circumferencial internal flaws in the SiC coating layer [7–10]. External observation was made of about 10,000 coated fuel particles after SiC deposition and the Triso-coated fuel particles from four fuel compacts, about 11,000 particles, burned back to the SiC coating layers. No discolored spot nor gold spot was observed on the SiC layers of total about 21,000 particles. Typical examples of the visual examination on the coated fuel particles after SiC deposition are shown in Fig. 3.5.

The coated fuel particles for the present irradiation test were fabricated after the optimization of the SiC coating process [8]; the internal flaws or the gold spots were mostly eliminated from the particles by controlling particle fluidization in the coater.

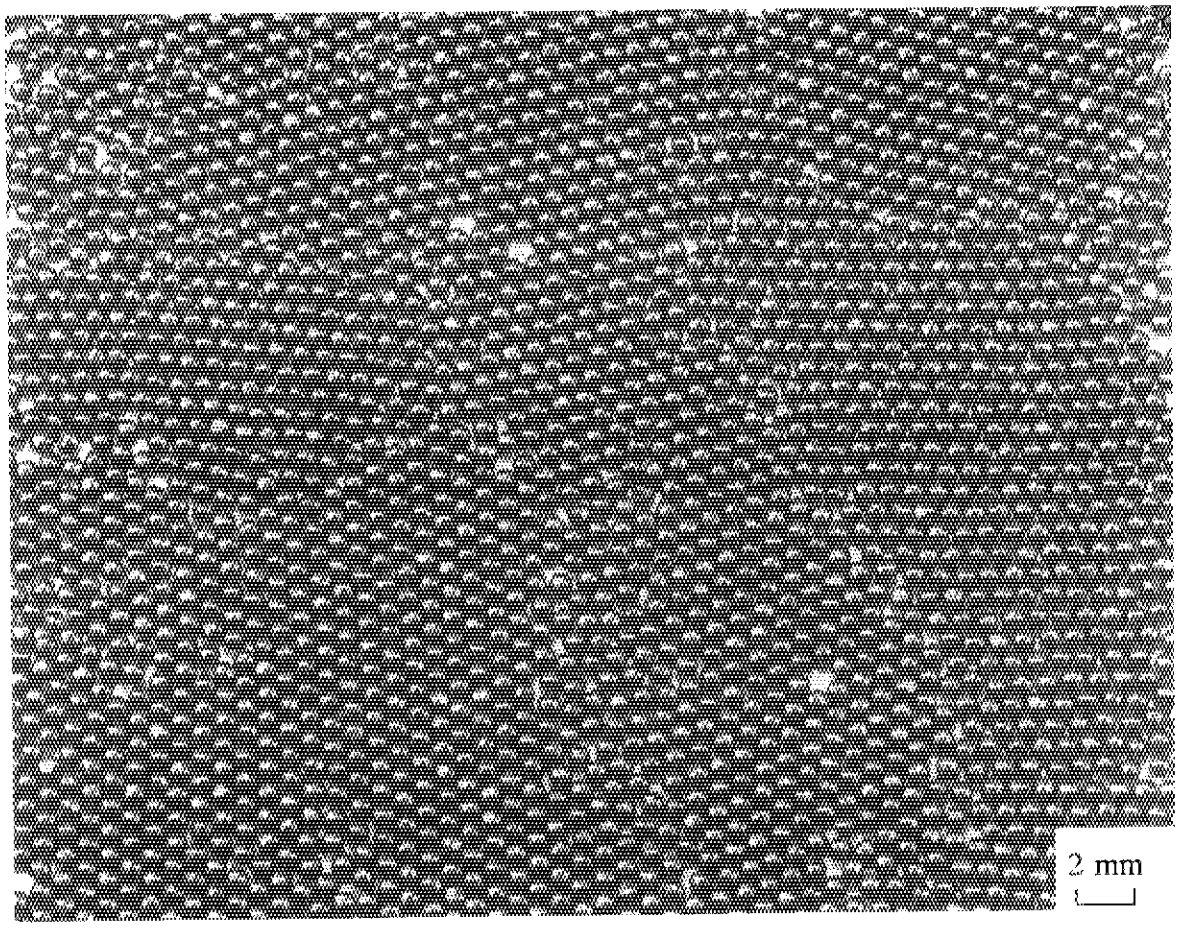

Fig. 3.5 Typical examples of external view of SiC-coated fuel particles.

3.2 *Characterization of Dummy Particles*

3.2.1 Dimensions of dummy particles

The diameter of the SiC-kernels with the IPyC layer and the thicknesses of the IPyC, SiC, and OPyC layers were measured on 100 particles by X-ray microradiography. The diameter of the dummy particles was measured on 929 particles by PSA. The results are shown in Table 3.6.

Table 3.6 Dimensions of dummy particles

	Mean (μm)
(Kernel+IPyC) diameter	761
IPyC thickness	14.9
SiC thickness	40.3
OPyC thickness	49.4
Particle diameter	929

3.2.2 Density of dummy particles

The densities of the IPyC and the SiC layers were measured on ten fragments of each layer by the sink-float method, and those of the OPyC layer and the dummy particle were measured on two samples of 2 g-particles by n-butanol pycnometry, as shown in Table 3.7.

Table 3.7 Density of dummy particles

	Mean (Mg/m^3)	Method
IPyC density	1.88	Sink-float method
SiC density	3.20	Sink-float method
OPyC density	1.82	n-butanol pycnometry
Particle density	2.13	n-butanol pycnometry

3.2.3 *External view of dummy particles*

As-fabricated dummy particles were observed by optical microscope. Typical examples are shown in Fig. 3.6.

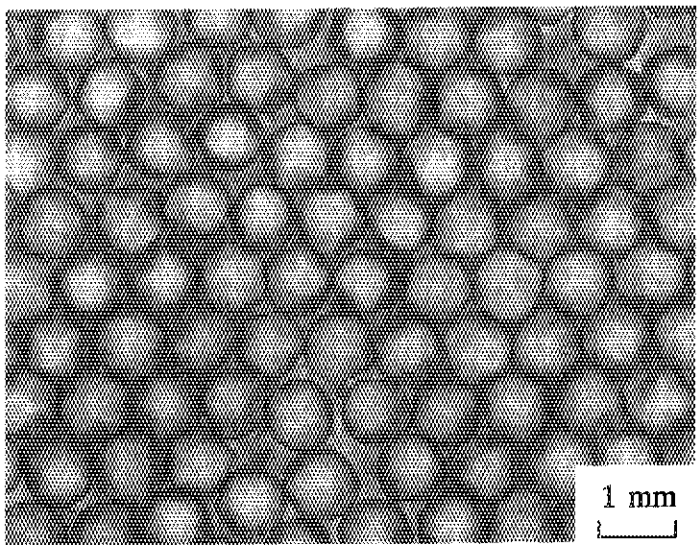

Fig. 3.6 External view of as-fabricated dummy particles.

3.2.4 *Ceramography of dummy particles*

The dummy particles were polished to their equators and observed by optical microscope. Typical examples are shown in Fig. 3.7.

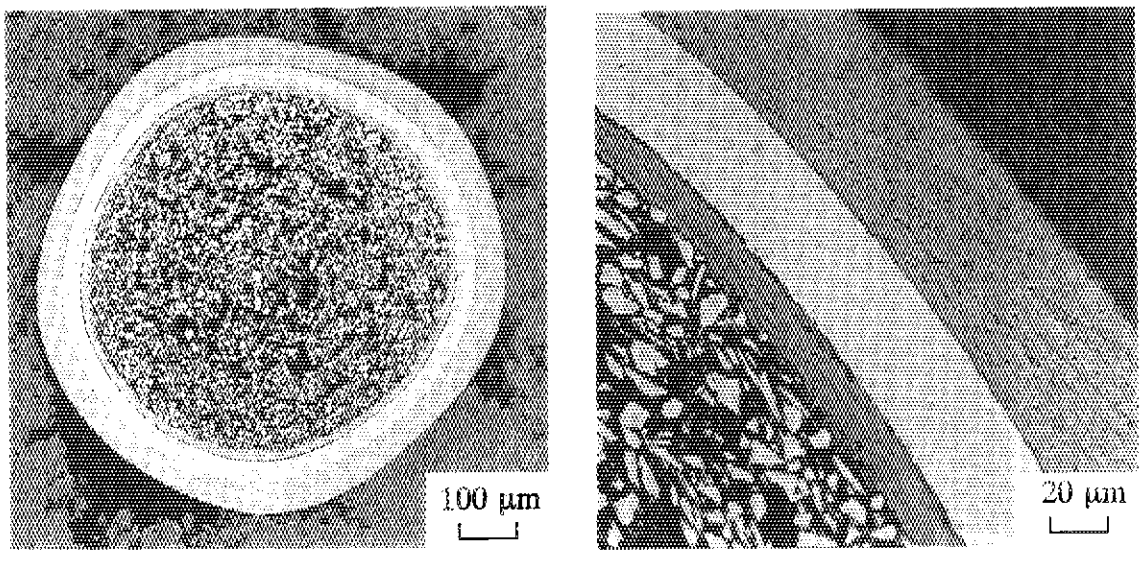

Fig. 3.7 Typical polished cross section of the dummy particle.

3.2.5 Internal flaws or gold spots of SiC layers

External observation was made of the dummy particles from four fuel compacts burned back to the SiC coating layers. A few percent of the particles had gold spots on the SiC layers. X-ray microradiography showed internal flaws in the SiC layers of the particles with gold spots. Figure 3.8 shows typical examples of the dummy particles with gold spots or internal flaws, which are the same kind as seen in the coated fuel particles fabricated before the optimization of the SiC coating process [8].

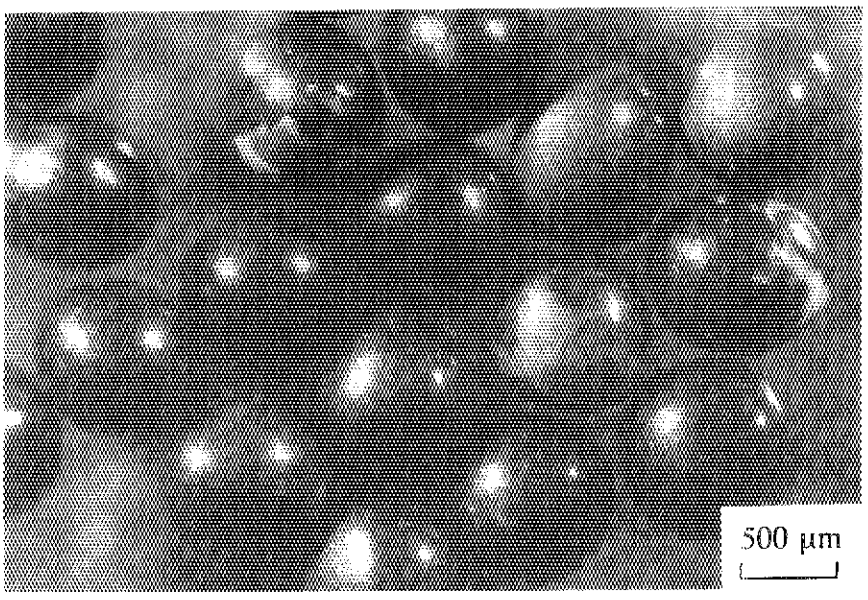

(a) Optical micrograph

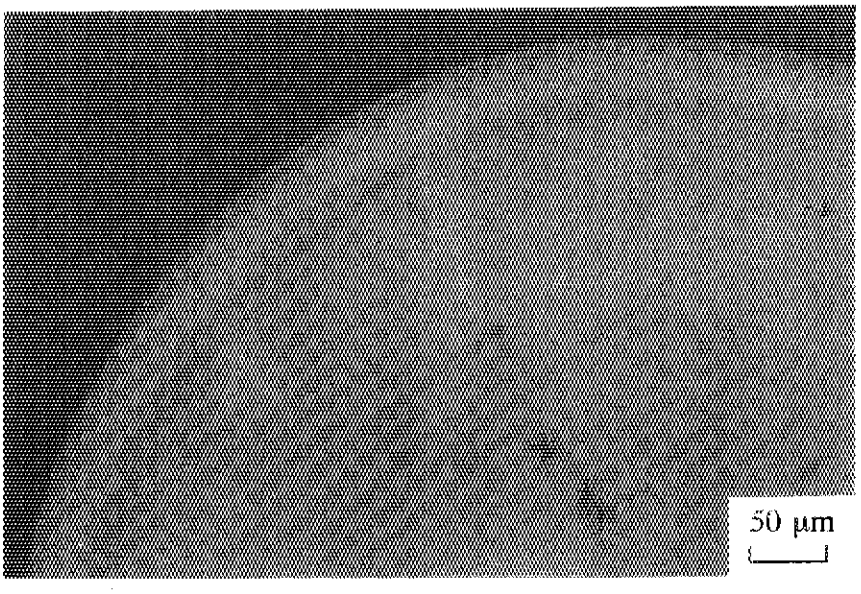

(b) X-ray microradiograph

Fig. 3.8 Typical examples of dummy particles with gold spots or internal flaws.

3.3 *Characterization of Fuel Compacts*

3.3.1 Dimensions of fuel compacts

An electromagnetic micrometer was used for measurement of the outer diameter and the length of the fuel compacts, and a micrometer for the inner diameter. The outer diameter was measured at six points of each fuel compact: at the top, middle and bottom of the compact in the two directions at right angles. The inner diameter was measured at two points of the top and the bottom of each compact. For the length, four points were sampled. The results are summarized in Table 3.8. All the measured values for 30 fuel compacts are listed in Appendix C.

Table 3.8 Dimensions of fuel compacts

	Range of values (mm)
Outer diameter	26.03 - 26.07
Inner diameter	10.00 - 10.02
Length	38.95 - 39.07

3.3.2 Weight and density of fuel compacts

The weight of the fuel compacts was measured by a direct reading balance. The density of the fuel compacts was calculated from the measured values of the weight and the dimensions. The results are summarized in Table 3.9. All the measured and calculated values for 30 fuel compacts are listed in Appendix D.

Table 3.9 Weight and density of fuel compacts

	Range of values
Weight (g)	34.244 - 34.327
Density (Mg/m^3)	1.93 - 1.94

3.3.3 *Packing fractions of particles*

The fuel compacts contained both the Triso-coated fuel particles and the dummy particles (SiC-kerneled coated particles). The packing fractions of these particles in the fuel compacts were calculated from the weight, the dimensions, and the fabrication data of the compacts. The results are summarized in Table 3.10. All the calculated values for 30 fuel compacts are listed in Appendix D.

Table 3.10 Packing fractions of particles

	Range of values (%)
Fuel particles	6.8
Dummy particles	27.1 – 27.2
Total	33.9 – 34.0

3.3.4 *Uranium content in fuel compacts*

The content of uranium in the fuel compacts was measured by γ-ray spectrometry. The measured values ranged from 2.260 to 2.371 g-U/compact. All the measured values for 30 fuel compacts are listed in Appendix D.

To check the uranium content in the fuel compacts, four fuel compacts were burned back to the SiC coating layers and the number of the fuel particles contained in each fuel

Table 3.11 Uranium content in fuel compacts

	Counting/calculation (g)	γ-ray spectrometry (g)
91OPB-5	2.27 (2821 particles)	2.300
91OPB-16	2.26 (2807 particles)	2.323
91OPB-20	2.26 (2807 particles)	2.331
91OPB-29	2.24 (2787 particles)	2.302

compact was counted with X-ray microradiography. The uranium content in each fuel compact was calculated from the mean uranium content in a fuel kernel and the number of the fuel particles contained in each fuel compact. The mean uranium content in a fuel kernel was calculated from the mean kernel diameter and the mean kernel density. The uranium content in the fuel compacts obtained by the counting/calculation method is listed in Table 3.11, where the results measured by the γ-ray spectrometry are also shown for comparison. It was found that the values obtained by the γ-ray spectrometry were systematically larger than those by the counting/calculation method by 2.5%.

3.3.5 Density of graphite matrix

The density of the graphite matrix of the fuel compacts was calculated from the weight, the dimensions, and the fabrication data of the compacts. The calculated values ranged from 1.68 to 1.69 Mg/m^3.

3.3.6 Free uranium fraction of fuel compacts

The free uranium fraction of the fuel compacts was measured by the deconsolidation followed by the acid leaching. Five fuel compacts were deconsolidated electrolytically and the deconsolidated samples were boiled in 7 mol/l nitric acid for 20 h, and the solution was analyzed for uranium by both fluorometric and colorimetric analyses. The measured values, as shown in Table 3.12, mean that no through-coating failure was present in the sampled fuel compacts, for about 2800 coated fuel particles were contained in a fuel compact.

Table 3.12 Free uranium fraction of coated fuel particles

	Fluorometric	Colorimetric
Sample C1	1.7×10^{-5}	3.6×10^{-5}
Sample C2	2.1×10^{-5}	5.3×10^{-5}
Sample C3	1.2×10^{-5}	2.9×10^{-5}
Sample C4	9.0×10^{-6}	2.2×10^{-5}
Sample C5	1.4×10^{-5}	3.1×10^{-5}

3.3.7 SiC-defective fraction of fuel compacts

The SiC-defective fraction of the fuel compacts was measured by two methods: by the burn/leach method and by the burn/X-ray microradiography.

In the burn/leach method, five fuel compacts were burned at 900°C in the air and the heating was continued for 6h after the OPyC layers were burned off. The burnt samples were boiled in 7 mol/l nitric acid for 5 h, and the solution was analyzed for uranium by both fluorometric and colorimetric analyses. The results are shown in Table 3.13. The measured values mean that no through-coating failure was present in the sampled fuel compacts, for about 2800 coated fuel particles were contained in a fuel compact.

Table 3.13 SiC-defective fraction of coated fuel particles by burn/leach method

	Fluorometric	Colorimetric
Sample D1	1.3×10^{-5}	1.1×10^{-5}
Sample D2	1.3×10^{-5}	1.1×10^{-5}
Sample D3	1.3×10^{-5}	1.1×10^{-5}
Sample D4	9.6×10^{-6}	9.3×10^{-6}
Sample D5	1.1×10^{-5}	1.0×10^{-5}

In the burn/X-ray microradiography, four fuel compacts were burned in the same manner as in the burn/leach method. The burnt samples were observed visually whether the SiC fragments and discolored particles were present or not. Before X-ray microradiography, the fuel particles were separated from the dummy particles using the density difference between them; the fuel particles sink in methylene iodide, while the dummy particles float. No SiC fragment was found in four sample. As described in sections 3.1.14 and 3.2.5, no gold spot was found on the SiC layers of the fuel particles, while a few percent of the dummy particles had gold spots on the SiC layers. With respect to the SiC-defective particle, a particle was found to be SiC-defective in the visual examination. Figure 3.9 shows the SiC-defective particle observed by optical microscopy and X-ray microradiography. The SiC-defective fractions of the coated fuel particles measured by the burn/X-ray microradiography are shown in Table 3.14.

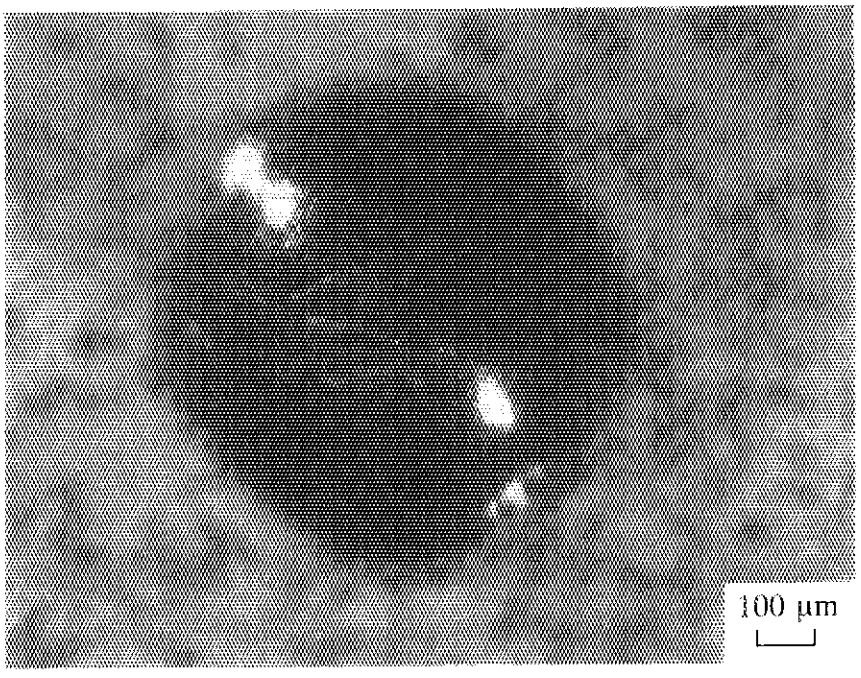

(a) Optical micrograph

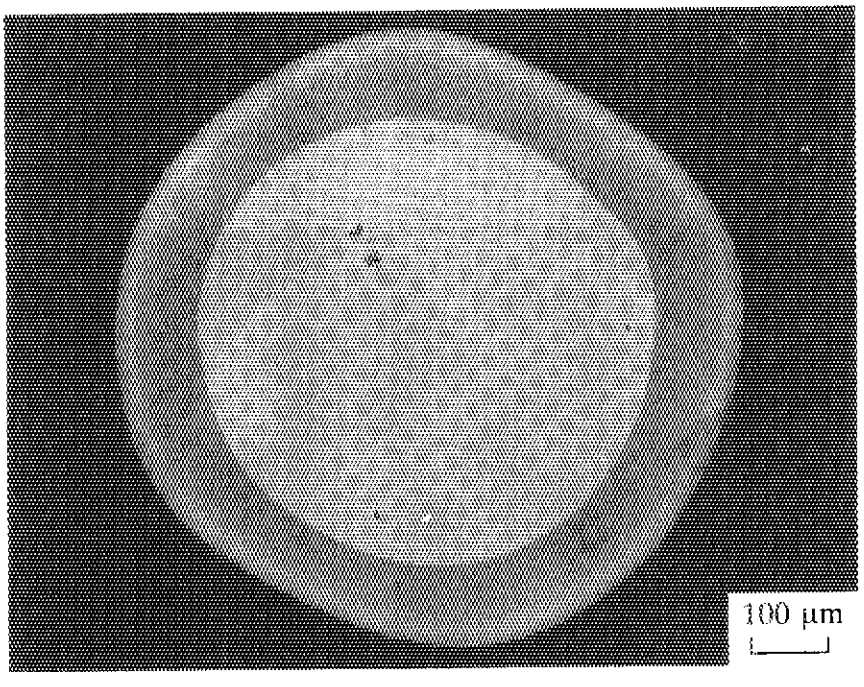

(b) X-ray microradiograph

Fig. 3.9 SiC-defective particle found in a fuel compact.

Table 3.14 SiC-defective fraction of coated fuel particles by burn/X-ray microradiography

	SiC-defective / Total particles
91OPB-5	0 / 2821
91OPB-16	0 / 2807
91OPB-20	0 / 2807
91OPB-29	1 / 2787 (3.6×10^{-4})

The SiC-defective particle was further observed by scanning electron microscopy. Figure 3.10 shows typical scanning electron micrographs of the SiC-defective particle.

As shown in Figs. 3.9 and 3.10, the cracks were observed on the surface of the SiC coating layer by optical microscopy and scanning electron microscopy. Although the X-ray microradiograph also showed the cracks, it revealed no anomaly in the fuel kernel, the buffer layer and the IPyC layer. If the cracks ran through the SiC layer, the buffer and the IPyC layers would be burned off and the UO_2 kernel would be oxidized to powder U_3O_8 during the burning of the fuel compact. From these facts, it was concluded that the cracks of the

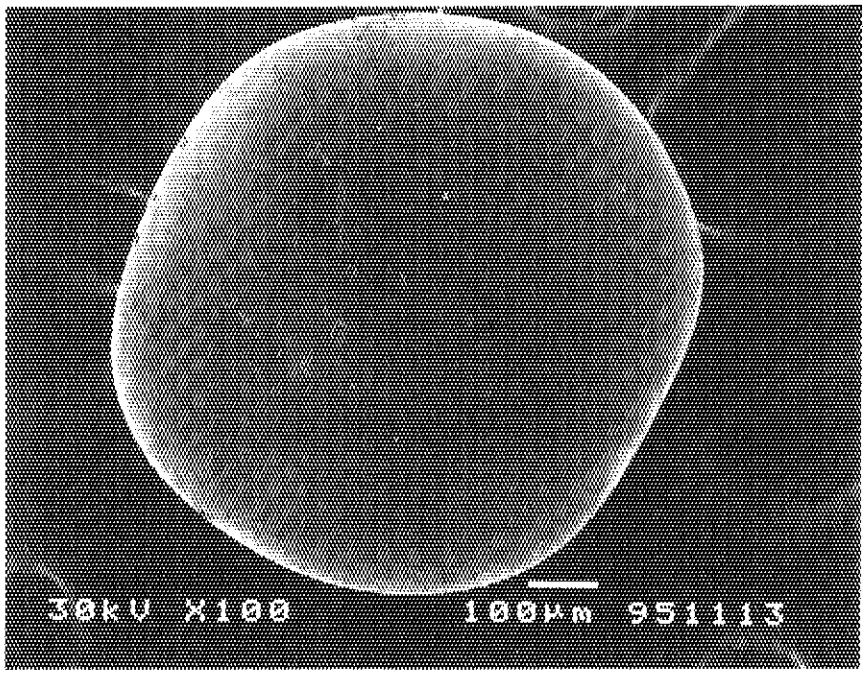

Fig. 3.10 Scanning electron micrographs of SiC-defective particle.

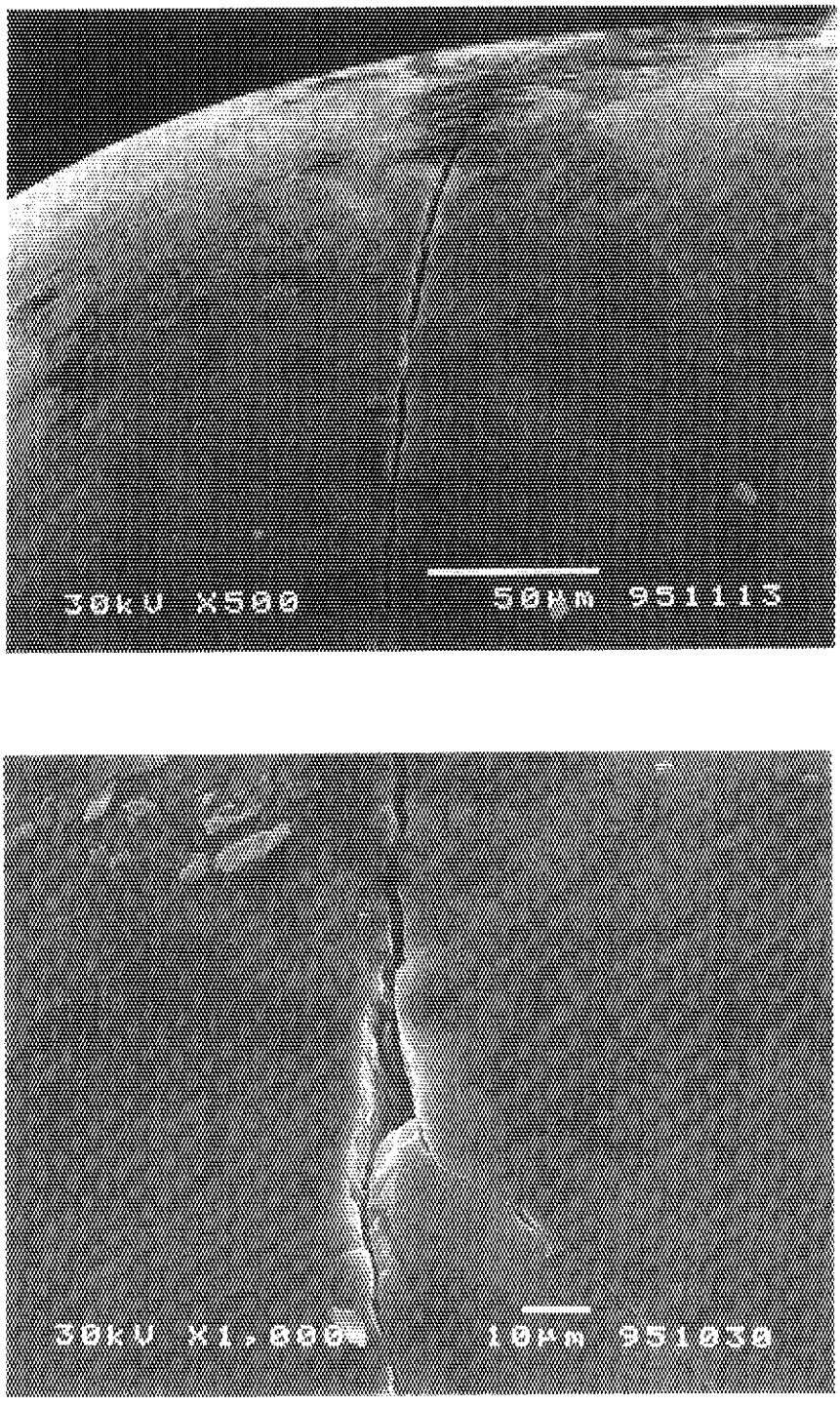

Fig. 3.10 Scanning electron micrographs of SiC-defective particle (continued).

SiC-defective particle found in 91OPB-29 fuel compact did not run through the SiC layer. The result of an additional heat treatment of the SiC-defective particle at 900°C for 6h confirmed this conclusion.

The mechanism for the formation of the SiC-defect of this kind was not determined. However, it must have been formed either after the SiC deposition by mechanical shocks or during the compact fabrication [6].

The SiC-defect of this kind is troublesome. It cannot be detected by the burn/leach method, which is usually applied to the determination of the SiC-defective fraction. The particles with the SiC-defect of this kind seem to have a high probability of the coating failure during irradiation.

3.3.8 Impurities in fuel compacts

The contents of 26 elements were analyzed in the fuel compacts. The results are summarized in Table 3.15.

Table 3.15 Impurities in fuel compacts

Element	Content (ppm)	Element	Content (ppm)
Ag	< 0.005	Gd	< 0.05
Al	3.0	K	< 0.7
B	0.08	Mg	< 0.09
Ca	18	Mo	0.4
Cd	0.02	N	< 0.2
Cl	< 0.2	Na	0.4
Cr	< 0.2	Ni	< 0.2
Cs	< 0.002	Pd	< 0.02
Cu	< 0.1	Ru	< 0.1
Dy	< 0.1	Si	2.4
Eu	< 0.0005	Sm	< 0.05
F	< 0.02	Ti	< 0.2
Fe	4.2	V	< 0.9

3.3.9 External view of fuel compacts

The externals of the fuel compacts were examined visually. On the top of each fuel compact, a mark of "S" was present. No anomaly was found, as shown in Fig. 3.11.

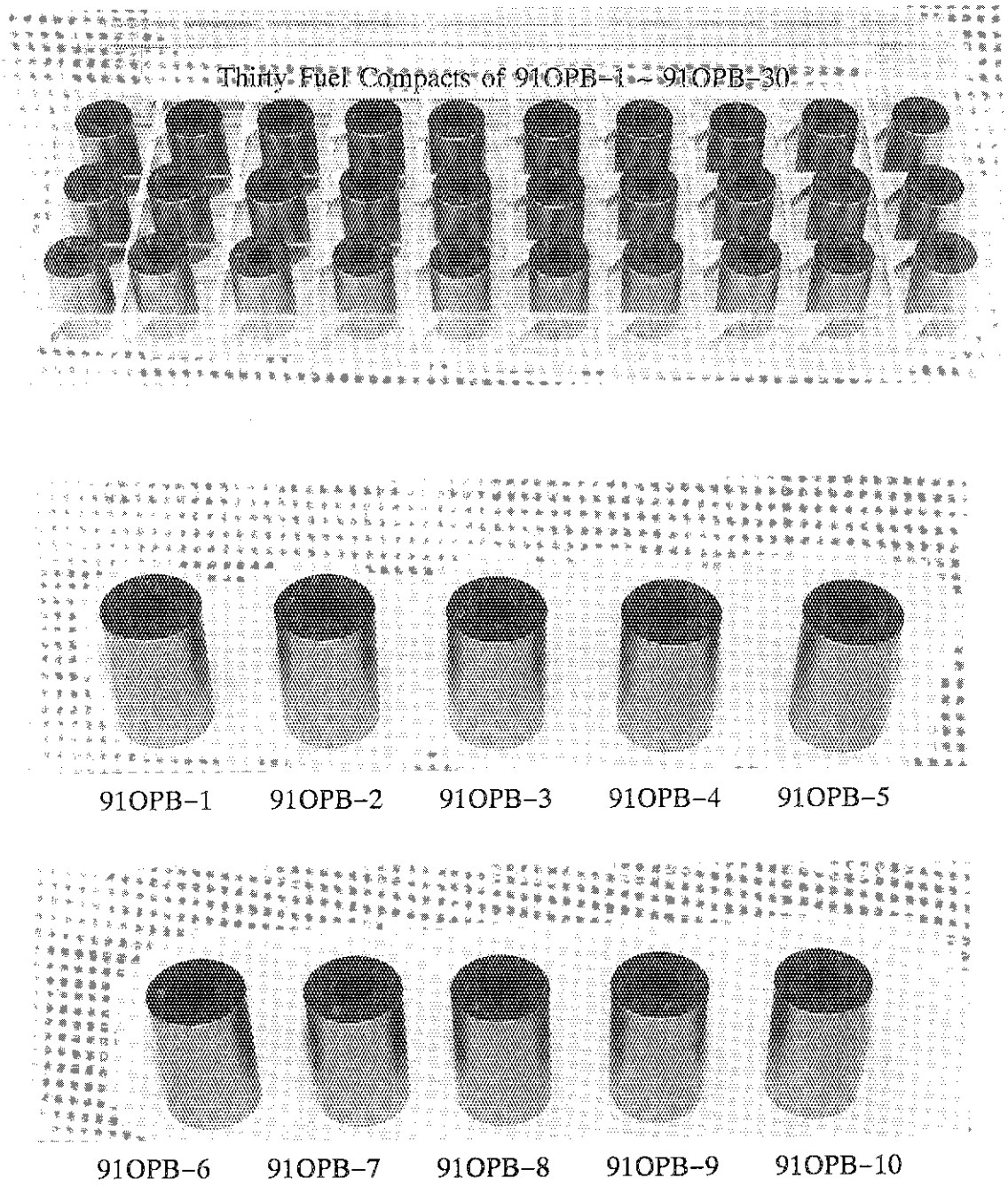

Fig. 3.11 External view of fuel compacts.

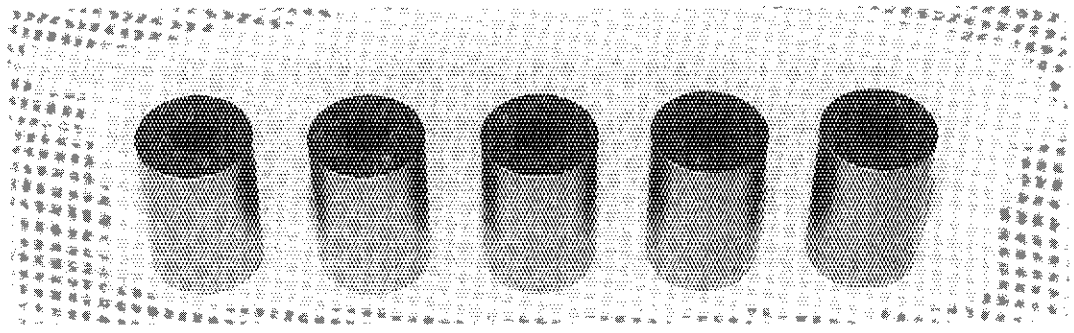

91OPB-11 91OPB-12 91OPB-13 91OPB-14 91OPB-15

91OPB-16 91OPB-17 91OPB-18 91OPB-19 91OPB-20

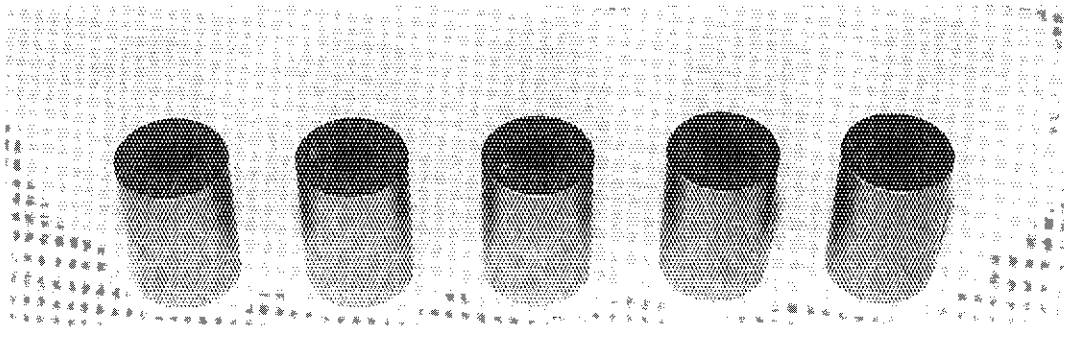

91OPB-21 91OPB-22 91OPB-23 91OPB-24 91OPB-25

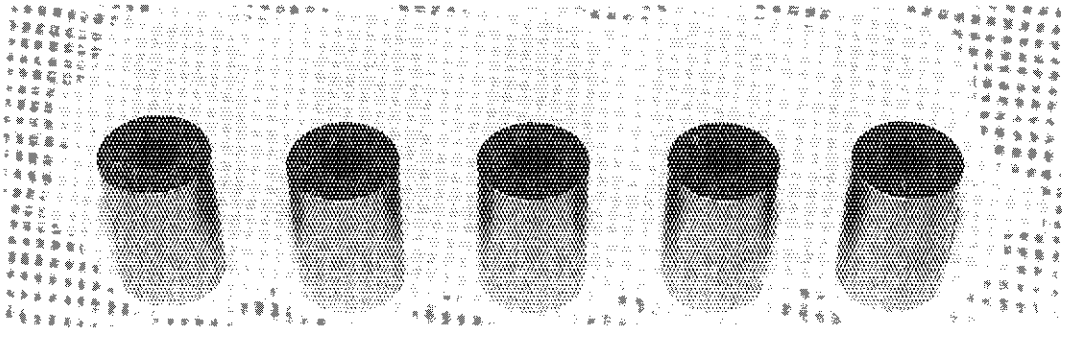

91OPB-26 91OPB-27 91OPB-28 91OPB-29 91OPB-30

Fig. 3.11 External view of fuel compacts (continued).

3.3.10 Ceramography of fuel compact

The fuel compact was polished and observed by optical microscope. No anomaly was found, as shown in Fig. 3.12.

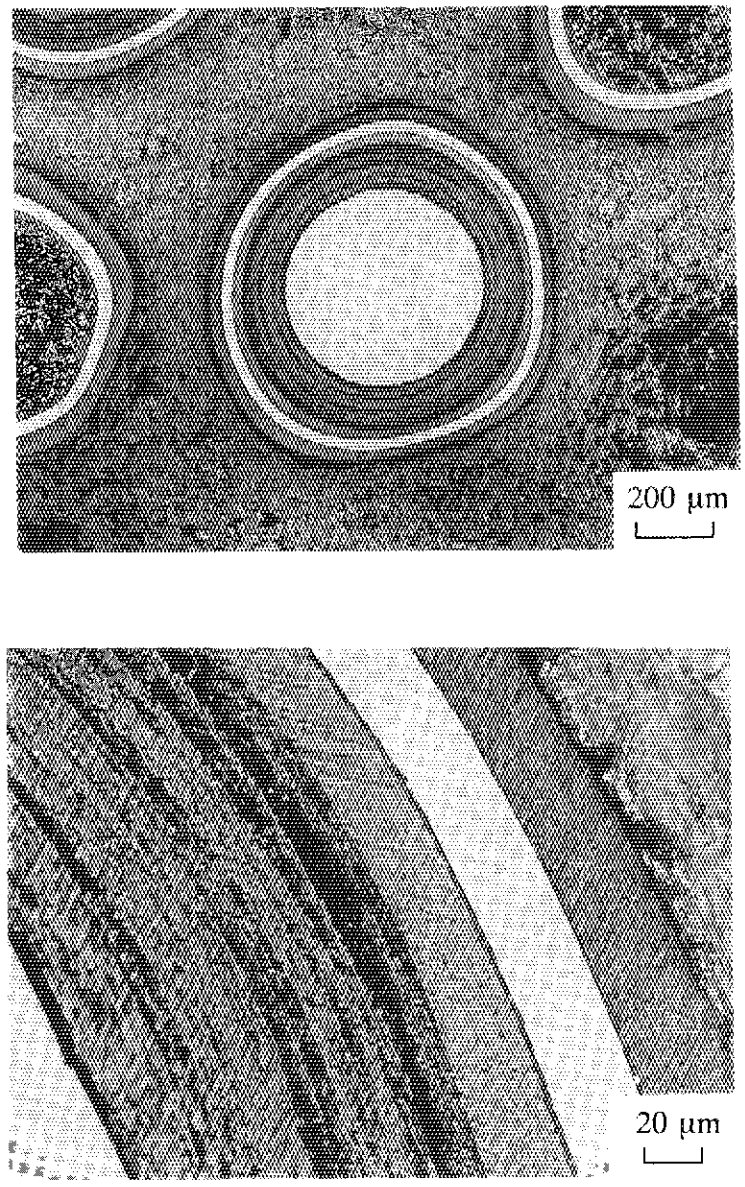

Fig. 3.12 Typical polished cross section of the fuel compact.

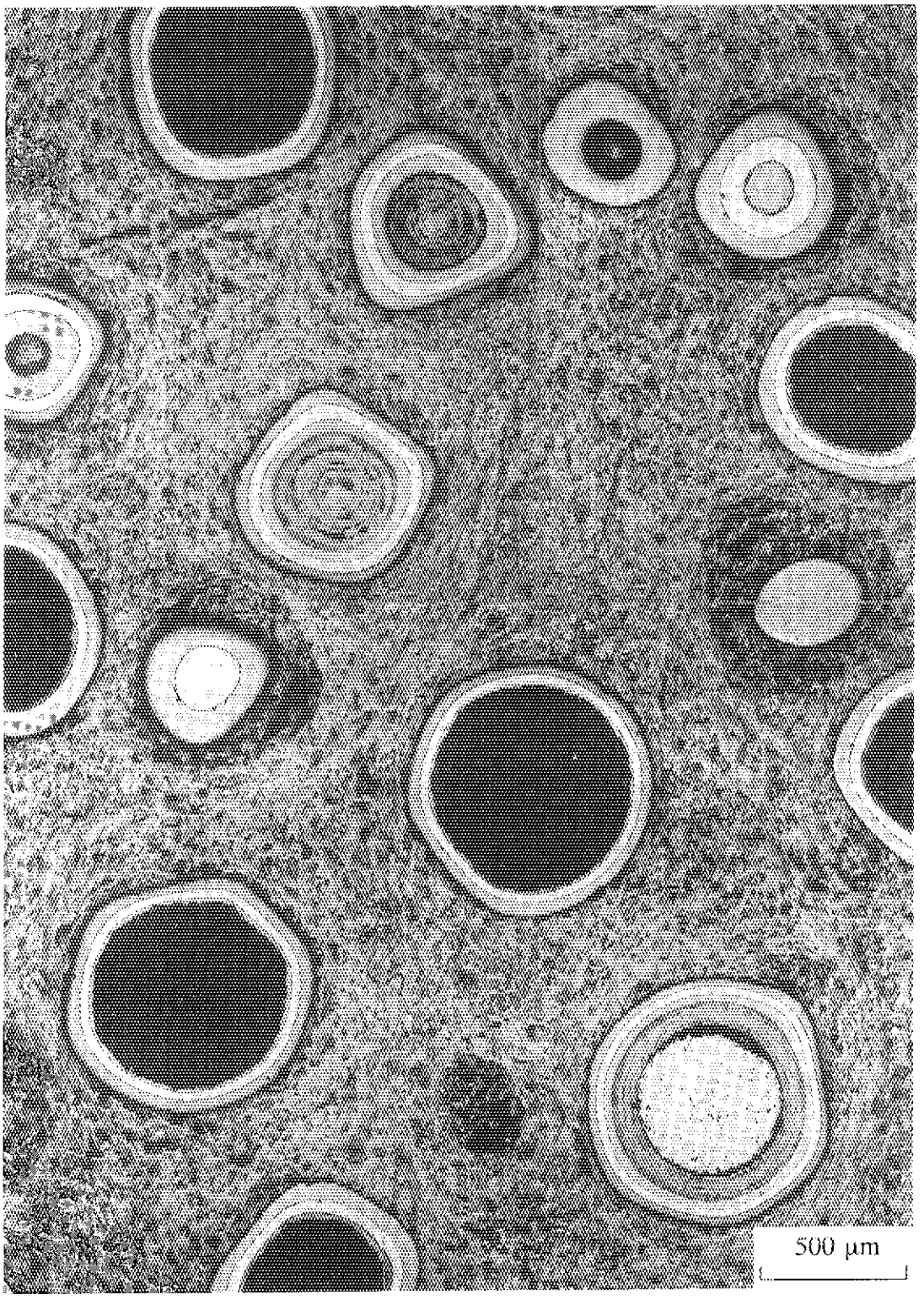

Fig. 3.12 Typical polished cross section of the fuel compact (continued).

4. SUMMARY

As a JAERI/USDOE collaborative irradiation test for high-temperature gas-cooled reactors fuel, HRB-22 capsule irradiation test of JAERI fuel compacts in HFIR followed by postirradiation examinations at ORNL was planed. The fuels loaded in the HRB-22 capsule were annular-shaped fuel compacts containing the Triso-coated fuel particles and the dummy particles. The dummy particles were needed to adjust a linear heat rate of the fuel.

The fuel design for the HRB-22 capsule irradiation test is called the advanced fuel, which is different from that for the initial core fuels of HTTR. A target burnup of the advanced fuel is 10 %FIMA, whereas that of the HTTR fuel is 3.6 %FIMA.

The UO_2 kernels of the fuel particles were fabricated by the gel-precipitation method. The coating layers of buffer, IPyC, SiC and OPyC were deposited on the kernels in the fluidized bed coater. The fuel compacts were fabricated by the overcoat/press method, where the Triso-coated fuel particles and the dummy particles were overcoated with graphite powder and pressed to form annular compacts.

The preirradiation characterization was performed of the Triso-coated fuel particles, the dummy particles and the fuel compacts. Measurements were made of the enrichment of U-235, the O/U ratio of the fuel kernels, the impurities in the fuel kernels, the dimensions of the coated fuel particles, the densities of the kernels and the coating layers, the OPTAF and the crystallite size of the PyC layers, the sphericity of the kernels and the coated fuel particles, the crushing strength of the coated fuel particles, the free uranium fraction of the coated fuel particles, the SiC-defective fraction of the coated fuel particles, the dimensions of the dummy particles, the density of the dummy particles, the dimensions of the fuel compacts, the weight and the density of the fuel compacts, the packing fraction of the particles, the uranium content in the fuel compacts, the density of the graphite matrix, the free uranium fraction of the fuel compacts, the SiC-defective fraction of the fuel compacts, and the impurities in the fuel compacts. Examinations were made of the external view of the coated fuel particles, the X-ray microradiography of the coated fuel particles, the ceramography of the coated fuel particles, the internal flaws or the gold spots of the SiC layers, the external view of the dummy particles, the ceramography of the dummy particles, the external view of the fuel compacts, and the ceramography of the fuel compacts.

The preirradiation characterization revealed that the fuels were suitable for the irradiation test and of good quality.

ACKNOWLEDGEMENTS

The authors wish to express their thanks to Dr. M. Hoshi, Director of the Department of Chemistry and Fuel Research, for his interest and encouragement.

REFERENCES

[1] K. Fukuda, T. Ogawa, K. Hayashi, S. Shiozawa, H. Tsuruta, I. Tanaka, N. Suzuki, S. Yoshimuta and M. Kaneko, Research and development of HTTR coated particle fuel, J. Nucl. Sci. Technol. 28 (1991) 570-581.

[2] S. Yoshimuta, N. Suzuki, M. Kaneko and K. Fukuda, Production process and quality control for the HTTR fuel, Proc. IAEA Specialists Meeting on Behaviour of Gas Cooled Reactor Fuel under Accident Conditions, Oak Ridge, USA, November 5-8, 1990 (IAEA,Vienna, 1991) pp. 37-42.

[3] S. Kashimura and K. Ikawa, Automatic size analysis of coated fuel particles, JAERI-M 84-196 (1984).

[4] HTGR Fuel Technology Program, Semiannual report for the period ending September 30, 1982, GA-A-16919 (1982).

[5] K. Minato, H. Kikuchi, and K. Fukuda, Detection of failed and defective coating layers in HTGR fuel particles by methylene iodide infusion, JAERI-M 87-024 (1987).

[6] K. Minato, H. Kikuchi, K. Fukuda, N. Suzuki, H. Tomimoto, N. Kitamura and M. Kaneko, Failure mechanisms of fuel particle coating for high-temperature gas-cooled reactors during the coating processes, Nucl. Technol. 111 (1995) 260.

[7] K. Minato, F. Kobayashi, H. Kikuchi, and K. Fukuda, Failure mechanisms of coated fuel particles during fabrication, JAERI-M 86-083 (1986).

[8] K. Minato, H. Kikuchi, K. Fukuda, N. Suzuki, H. Tomimoto, N. Kitamura and M. Kaneko, Internal flaws in the silicon carbide coating of fuel particles for high-temperature gas-cooled reactor, Nucl. Technol. 106 (1994) 342.

[9] HTGR Fuel Technology Program, Semiannual report for the period ending March 31, 1984, GA-A-17612 (1984).

[10] M. J. Kania, Capsule HRB-21 postirradiation examination, Personal communication, Oak Ridge National Laboratory (1993).

ACKNOWLEDGEMENTS

The authors wish to express their thanks to Dr. M. Hoshi, Director of the Department of Chemistry and Fuel Research, for his interest and encouragement.

REFERENCES

[1] K. Fukuda, T. Ogawa, K. Hayashi, S. Shiozawa, H. Tsuruta, I. Tanaka, N. Suzuki, S. Yoshimuta and M. Kaneko, Research and development of HTTR coated particle fuel, J. Nucl. Sci. Technol. 28 (1991) 570–581.

[2] S. Yoshimuta, N. Suzuki, M. Kaneko and K. Fukuda, Production process and quality control for the HTTR fuel, Proc. IAEA Specialists Meeting on Behaviour of Gas Cooled Reactor Fuel under Accident Conditions, Oak Ridge, USA, November 5–8, 1990 (IAEA,Vienna, 1991) pp. 37–42.

[3] S. Kashimura and K. Ikawa, Automatic size analysis of coated fuel particles, JAERI–M 84–196 (1984).

[4] HTGR Fuel Technology Program, Semiannual report for the period ending September 30, 1982, GA–A–16919 (1982).

[5] K. Minato, H. Kikuchi, and K. Fukuda, Detection of failed and defective coating layers in HTGR fuel particles by methylene iodide infusion, JAERI–M 87–024 (1987).

[6] K. Minato, H. Kikuchi, K. Fukuda, N. Suzuki, H. Tomimoto, N. Kitamura and M. Kaneko, Failure mechanisms of fuel particle coating for high–temperature gas–cooled reactors during the coating processes, Nucl. Technol. 111 (1995) 260.

[7] K. Minato, F. Kobayashi, H. Kikuchi, and K. Fukuda, Failure mechanisms of coated fuel particles during fabrication, JAERI–M 86–083 (1986).

[8] K. Minato, H. Kikuchi, K. Fukuda, N. Suzuki, H. Tomimoto, N. Kitamura and M. Kaneko, Internal flaws in the silicon carbide coating of fuel particles for high–temperature gas–cooled reactor, Nucl. Technol. 106 (1994) 342.

[9] HTGR Fuel Technology Program, Semiannual report for the period ending March 31, 1984, GA–A–17612 (1984).

[10] M. J. Kania, Capsule HRB–21 postirradiation examination, Personal communication, Oak Ridge National Laboratory (1993).

APPENDIX A COATING THICKNESSES OF FUEL PARTICLES

Table A.1 Buffer layer thicknesses (mean of four measured values in a particle)

No.	Thickness (μm)	No.	Thickness (μm)	No.	Thickness (μm)	No.	Thickness (μm)
1	116.00	51	92.25	101	196.25	151	112.00
2	84.00	52	95.75	102	99.75	152	106.75
3	67.25	53	88.50	103	103.50	153	92.75
4	93.50	54	103.25	104	85.00	154	111.25
5	111.75	55	99.50	105	73.50	155	105.50
6	97.00	56	99.50	106	103.50	156	102.25
7	94.75	57	109.75	107	109.50	157	98.25
8	110.25	58	114.25	108	74.25	158	108.25
9	106.75	59	102.25	109	119.50	159	86.25
10	95.00	60	79.00	110	82.75	160	73.75
11	108.00	61	75.50	111	90.75	161	81.00
12	101.25	62	88.50	112	106.75	162	75.00
13	100.50	63	108.75	113	93.25	163	79.50
14	88.50	64	97.75	114	102.25	164	89.75
15	109.00	65	108.50	115	111.50	165	112.00
16	83.25	66	103.25	116	97.50	166	89.25
17	91.00	67	91.00	117	82.75	167	91.25
18	86.00	68	68.75	118	90.50	168	94.75
19	89.25	69	99.75	119	112.25	169	80.75
20	99.50	70	108.50	120	107.25	170	104.00
21	99.50	71	92.50	121	72.50	171	98.00
22	109.00	72	100.00	122	106.50	172	97.75
23	124.25	73	128.00	123	90.75	173	90.00
24	79.50	74	96.75	124	119.50	174	90.25
25	95.50	75	99.50	125	99.75	175	120.00
26	78.50	76	87.75	126	95.00	176	83.25
27	111.00	77	97.75	127	90.25	177	101.00
28	80.00	78	119.50	128	86.25	178	85.00
29	79.00	79	111.00	129	93.00	179	106.25
30	106.50	80	97.00	130	98.25	180	94.50
31	88.75	81	100.75	131	95.25	181	93.25
32	93.00	82	103.25	132	117.50	182	90.75
33	109.25	83	82.50	133	107.25	183	108.75
34	88.25	84	103.50	134	73.25	184	110.00
35	110.25	85	88.50	135	110.50	185	103.50
36	90.00	86	89.75	136	86.25	186	127.25
37	76.75	87	101.25	137	128.25	187	98.25
38	76.75	88	93.25	138	66.75	188	60.25
39	76.00	89	90.25	139	83.25	189	76.50
40	103.25	90	88.25	140	113.75	190	92.00
41	121.75	91	103.25	141	92.75	191	90.25
42	103.75	92	104.50	142	88.25	192	92.75
43	98.50	93	112.50	143	114.25	193	110.25
44	108.25	94	88.50	144	81.50	194	97.25
45	91.50	95	99.50	145	125.50	195	115.50
46	109.25	96	97.00	146	96.00	196	94.50
47	101.50	97	96.25	147	91.00	197	88.00
48	108.50	98	96.25	148	125.75	198	83.25
49	97.00	99	95.75	149	106.50	199	118.25
50	104.25	100	105.50	150	101.75	200	106.25

Table A.2 IPyC layer thicknesses (mean of four measured values in a particle)

No.	Thickness (μm)	No.	Thickness (μm)	No.	Thickness (μm)	No.	Thickness (μm)
1	31.00	51	31.00	101	28.00	151	32.50
2	33.25	52	35.75	102	38.75	152	36.50
3	35.25	53	27.50	103	31.75	153	29.50
4	29.75	54	36.25	104	32.50	154	36.00
5	31.25	55	31.00	105	35.50	155	28.25
6	28.75	56	29.75	106	29.50	156	31.25
7	33.00	57	39.00	107	34.25	157	35.00
8	37.50	58	41.75	108	35.00	158	33.75
9	26.00	59	31.00	109	34.50	159	31.00
10	29.00	60	32.25	110	38.50	160	30.50
11	31.50	61	33.25	111	28.25	161	35.25
12	35.75	62	33.00	112	34.50	162	32.25
13	26.25	63	34.75	113	31.75	163	31.50
14	36.25	64	32.50	114	29.25	164	33.75
15	31.50	65	30.50	115	38.00	165	31.00
16	38.25	66	32.50	116	32.25	166	30.50
17	35.00	67	35.25	117	31.25	167	27.50
18	38.75	68	34.50	118	33.25	168	29.00
19	25.00	69	35.25	119	36.50	169	33.00
20	40.50	70	32.25	120	29.25	170	28.75
21	37.50	71	29.00	121	33.25	171	37.00
22	37.25	72	36.00	122	27.75	172	35.25
23	38.50	73	35.75	123	35.25	173	33.50
24	38.75	74	32.25	124	32.00	174	33.00
25	32.00	75	35.25	125	30.25	175	33.50
26	30.00	76	34.00	126	31.00	176	38.25
27	31.75	77	34.00	127	36.00	177	32.50
28	32.75	78	40.00	128	31.00	178	33.75
29	36.00	79	32.25	129	37.25	179	36.75
30	35.25	80	26.25	130	32.75	180	30.00
31	38.00	81	34.50	131	25.00	181	27.25
32	38.75	82	27.75	132	34.50	182	31.50
33	27.75	83	28.50	133	34.50	183	31.00
34	33.25	84	26.00	134	32.50	184	30.75
35	35.00	85	35.75	135	28.75	185	32.75
36	32.25	86	33.25	136	31.00	186	30.50
37	33.50	87	28.75	137	30.50	187	37.00
38	28.25	88	25.75	138	33.25	188	28.50
39	38.25	89	28.50	139	32.00	189	35.50
40	31.50	90	32.25	140	29.50	190	27.00
41	36.50	91	31.50	141	31.75	191	34.75
42	32.50	92	34.75	142	31.50	192	31.25
43	35.00	93	33.50	143	33.50	193	35.25
44	33.00	94	43.00	144	30.00	194	38.00
45	28.75	95	30.75	145	31.00	195	32.50
46	28.75	96	33.00	146	36.50	196	29.50
47	33.75	97	28.00	147	34.75	197	36.00
48	37.50	98	36.75	148	31.50	198	35.25
49	37.75	99	31.75	149	31.25	199	29.50
50	30.00	100	38.00	150	36.50	200	31.75

Table A.3 SiC layer thicknesses (mean of four measured values in a particle)

No.	Thickness (μm)	No.	Thickness (μm)	No.	Thickness (μm)	No.	Thickness (μm)
1	31.00	51	31.25	101	35.00	151	36.25
2	33.25	52	31.50	102	33.75	152	33.50
3	30.75	53	33.25	103	32.75	153	33.25
4	31.50	54	33.25	104	35.75	154	34.25
5	32.75	55	34.00	105	34.25	155	33.00
6	31.00	56	33.25	106	32.25	156	32.25
7	37.75	57	32.00	107	33.00	157	35.50
8	31.25	58	34.50	108	34.00	158	32.50
9	33.75	59	34.75	109	34.50	159	35.25
10	34.50	60	34.75	110	31.25	160	32.25
11	35.25	61	33.00	111	33.50	161	31.75
12	34.00	62	33.75	112	34.00	162	33.75
13	33.00	63	33.75	113	32.75	163	33.25
14	31.25	64	32.25	114	34.50	164	34.00
15	33.50	65	33.00	115	31.75	165	33.75
16	32.25	66	34.00	116	34.25	166	33.50
17	32.50	67	34.75	117	32.50	167	33.25
18	32.25	68	35.00	118	34.00	168	32.75
19	33.75	69	35.00	119	34.25	169	31.25
20	33.25	70	36.00	120	34.00	170	33.25
21	34.50	71	31.25	121	33.50	171	31.75
22	32.75	72	33.00	122	33.00	172	33.00
23	34.25	73	33.50	123	33.75	173	34.00
24	32.75	74	33.00	124	33.50	174	35.50
25	34.00	75	33.00	125	35.25	175	35.50
26	32.50	76	34.50	126	35.25	176	34.50
27	36.75	77	33.75	127	34.75	177	34.00
28	33.25	78	34.00	128	36.25	178	32.00
29	33.75	79	32.75	129	32.75	179	36.50
30	32.50	80	34.00	130	33.00	180	34.75
31	32.75	81	31.50	131	35.75	181	36.25
32	39.25	82	32.25	132	33.75	182	34.50
33	31.00	83	33.00	133	34.25	183	36.00
34	33.50	84	32.25	134	33.75	184	32.00
35	34.25	85	35.50	135	32.50	185	33.00
36	34.75	86	33.50	136	29.50	186	36.75
37	37.00	87	33.75	137	34.50	187	35.75
38	31.25	88	32.25	138	35.50	188	36.75
39	31.25	89	35.25	139	33.50	189	34.25
40	30.25	90	35.25	140	33.50	190	38.25
41	33.25	91	34.75	141	34.75	191	36.75
42	32.25	92	31.75	142	32.75	192	35.25
43	31.75	93	34.75	143	35.50	193	31.25
44	35.00	94	32.75	144	35.75	194	32.50
45	34.75	95	35.75	145	33.75	195	36.00
46	34.00	96	34.75	146	33.75	196	36.75
47	33.00	97	33.75	147	30.25	197	31.25
48	32.50	98	34.50	148	33.25	198	34.75
49	32.75	99	31.75	149	34.75	199	34.25
50	30.75	100	34.50	150	34.75	200	37.50

Table A.4 OPyC layer thicknesses (mean of four measured values in a particle)

No.	Thickness (μm)	No.	Thickness (μm)	No.	Thickness (μm)	No.	Thickness (μm)
1	42.75	51	36.75	101	43.50	151	42.25
2	36.75	52	36.00	102	42.00	152	39.00
3	39.00	53	33.25	103	43.25	153	31.50
4	39.75	54	36.00	104	42.00	154	35.75
5	41.50	55	34.00	105	42.00	155	37.00
6	37.50	56	39.00	106	41.75	156	39.50
7	37.00	57	31.50	107	40.00	157	41.25
8	37.50	58	38.00	108	42.75	158	39.00
9	39.50	59	37.00	109	43.25	159	37.50
10	39.50	60	41.75	110	44.25	160	45.00
11	41.25	61	35.50	111	37.50	161	39.50
12	38.50	62	39.50	112	35.75	162	41.75
13	45.50	63	34.75	113	38.50	163	42.00
14	45.50	64	41.25	114	37.25	164	44.50
15	36.75	65	37.75	115	41.00	165	39.50
16	31.00	66	35.25	116	40.25	166	39.75
17	35.75	67	38.00	117	40.75	167	43.00
18	41.75	68	29.50	118	39.75	168	40.75
19	41.00	69	32.25	119	36.00	169	42.75
20	37.75	70	39.00	120	39.25	170	36.75
21	36.00	71	38.50	121	38.75	171	36.75
22	43.75	72	38.25	122	39.75	172	42.00
23	34.75	73	39.25	123	37.50	173	41.25
24	30.75	74	41.50	124	40.00	174	43.00
25	45.00	75	39.00	125	42.00	175	45.50
26	37.25	76	38.75	126	40.00	176	40.75
27	39.50	77	41.00	127	34.50	177	40.50
28	39.25	78	42.00	128	37.50	178	39.50
29	36.25	79	42.50	129	34.50	179	39.00
30	42.25	80	37.00	130	38.75	180	35.00
31	39.00	81	40.75	131	42.00	181	38.75
32	43.00	82	40.25	132	38.00	182	34.50
33	37.25	83	44.25	133	41.75	183	42.25
34	33.75	84	45.25	134	41.25	184	40.25
35	36.50	85	39.50	135	42.25	185	39.50
36	36.50	86	40.25	136	40.75	186	37.25
37	41.25	87	42.00	137	38.75	187	36.00
38	38.25	88	44.00	138	43.50	188	38.00
39	41.00	89	40.50	139	40.25	189	38.75
40	38.50	90	36.00	140	45.25	190	43.25
41	35.50	91	34.50	141	41.75	191	38.00
42	42.50	92	38.75	142	41.25	192	38.00
43	42.25	93	37.00	143	41.50	193	41.00
44	41.50	94	33.25	144	40.75	194	33.75
45	37.75	95	40.00	145	44.25	195	41.50
46	36.50	96	36.75	146	44.50	196	38.75
47	37.25	97	38.75	147	45.50	197	36.50
48	39.75	98	41.25	148	37.75	198	38.25
49	40.25	99	39.50	149	35.50	199	38.75
50	42.00	100	41.50	150	40.00	200	39.50

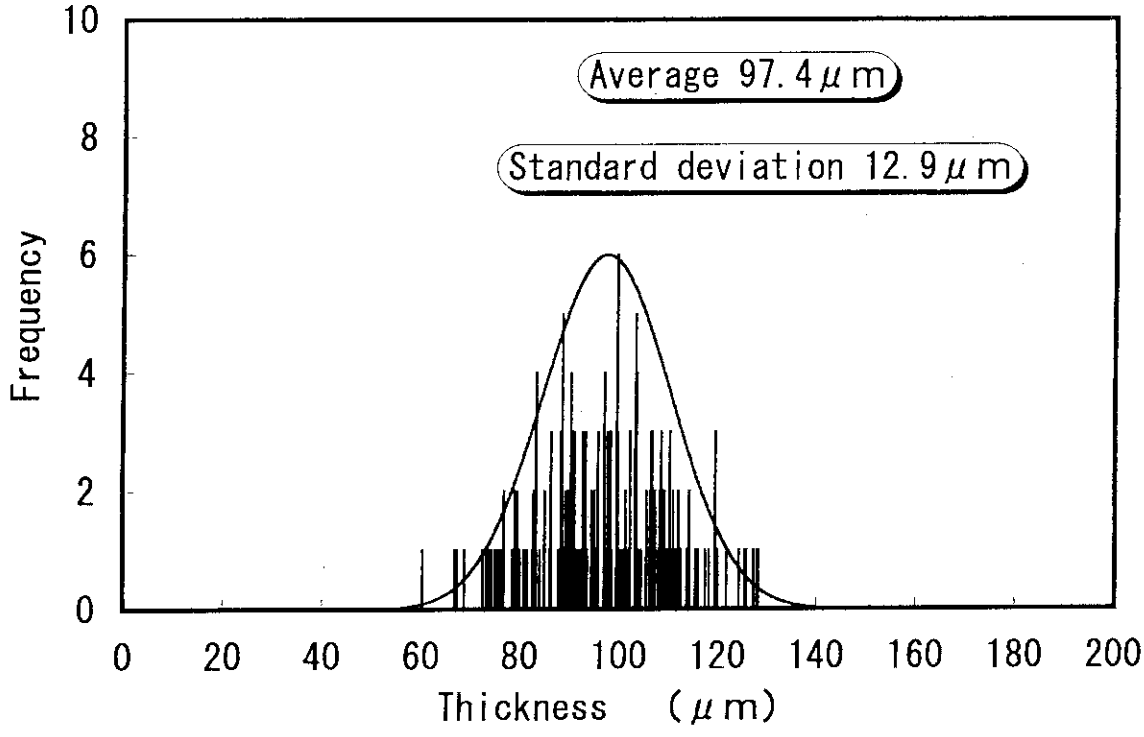

Fig. A.1 Distribution of buffer layer thicknesses

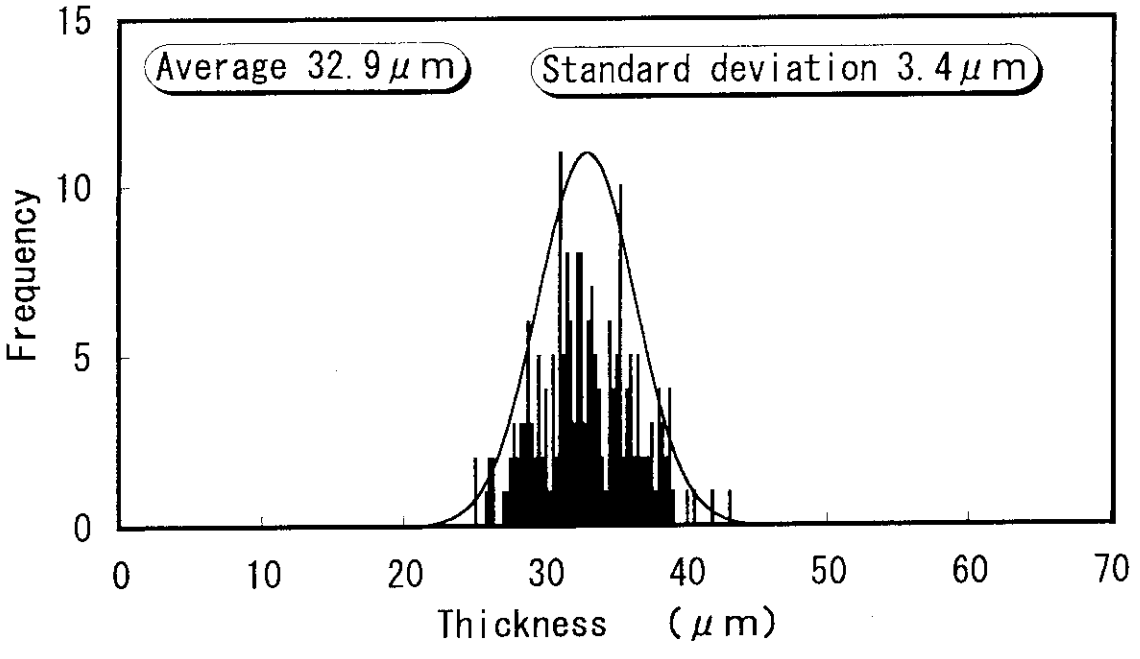

Fig. A.2 Distribution of IPyC layer thicknesses

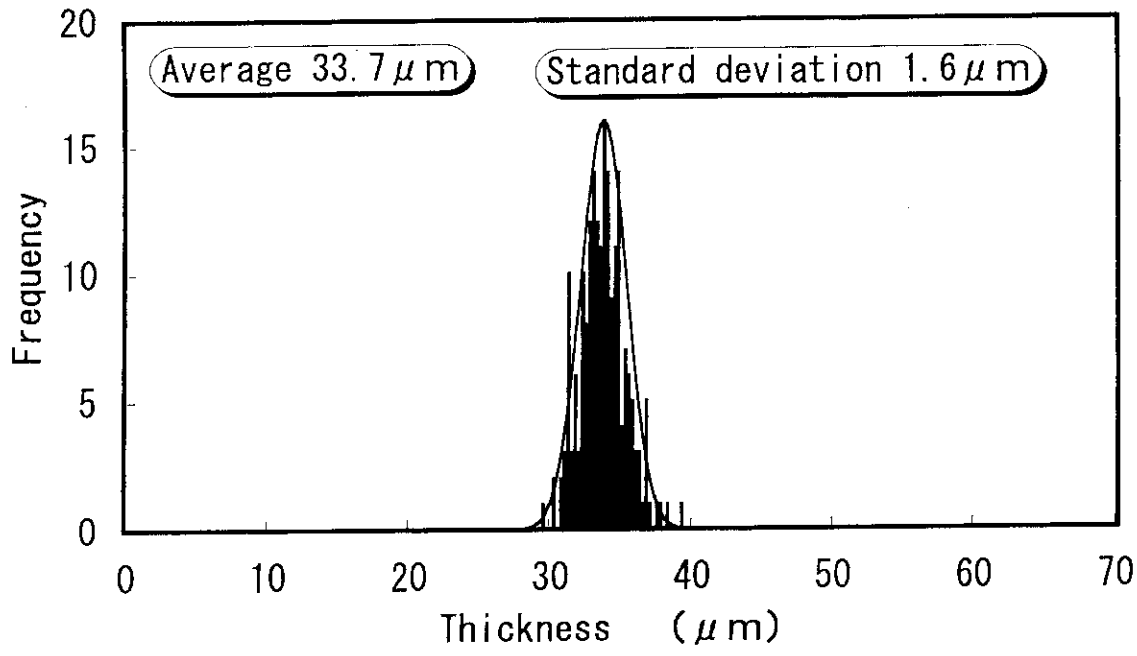

Fig. A.3 Distribution of SiC layer thicknesses

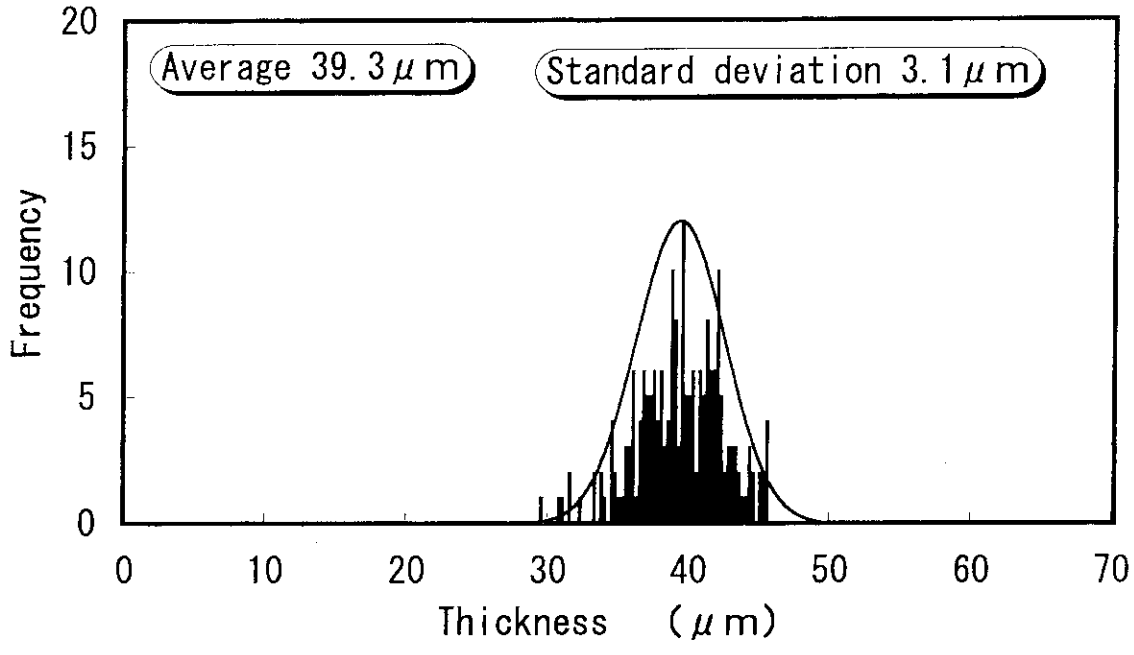

Fig. A.4 Distribution of OPyC layer thicknesses

APPENDIX B CRUSHING STRENGTH OF COATED FUEL PARTICLES

Table B.1 Crushing strength of Triso-coated fuel particles

No.	Strength (N)	No.	Strength (N)
1	17.65	26	18.53
2	21.77	27	21.18
3	20.30	28	20.59
4	17.65	29	19.42
5	25.01	30	21.48
6	20.01	31	20.01
7	19.71	32	20.30
8	26.48	33	20.30
9	26.48	34	26.77
10	32.36	35	24.71
11	21.48	36	27.36
12	21.18	37	19.71
13	24.71	38	25.89
14	26.18	39	28.83
15	26.48	40	23.54
16	25.89	41	20.89
17	21.18	42	20.30
18	19.12	43	19.42
19	29.42	44	27.36
20	21.48	45	18.24
21	20.30	46	30.89
22	20.59	47	23.24
23	26.77	48	24.71
24	23.54	49	19.71
25	24.71	50	20.30

APPENDIX C DIMENSIONS OF FUEL COMPACTS

Table C.1 Dimensions of fuel compacts loaded in HRB-22 capsule

Name	Outer diameter (mm)			Inner diameter (mm)		Length (mm)	
	top	middle	bottom	top	bottom		
91OPB-2	26.05	26.05	26.06	10.01	10.02	39.01	38.98
	26.04	26.05	26.06			38.96	38.97
91OPB-3	26.04	26.05	26.05	10.01	10.01	39.01	39.00
	26.05	26.05	26.05			38.99	39.00
91OPB-7	26.03	26.04	26.05	10.00	10.01	39.03	39.01
	26.04	26.05	26.06			38.99	39.00
91OPB-8	26.04	26.04	26.05	10.01	10.01	39.02	38.98
	26.05	26.05	26.05			38.97	38.99
91OPB-9	26.05	26.04	26.05	10.01	10.01	39.03	39.02
	26.04	26.05	26.05			38.99	39.02
91OPB-10	26.04	26.05	26.05	10.01	10.02	39.01	38.99
	26.04	26.06	26.06			39.01	39.02
91OPB-11	26.04	26.05	26.05	10.01	10.02	39.02	39.02
	26.04	26.05	26.05			39.01	39.02
91OPB-12	26.04	26.05	26.05	10.01	10.01	39.02	39.01
	26.05	26.05	26.06			39.00	39.01
91OPB-15	26.04	26.04	26.06	10.00	10.02	39.00	39.00
	26.03	26.05	26.05			38.98	38.99
91OPB-17	26.04	26.05	26.05	10.02	10.02	39.01	39.01
	26.04	26.05	26.05			39.00	38.99
91OPB-21	26.03	26.04	26.06	10.00	10.02	39.04	39.04
	26.04	26.06	26.05			39.02	38.99
91OPB-22	26.05	26.05	26.06	10.02	10.01	39.00	39.00
	26.05	26.05	26.05			39.00	38.99

Table C.2 Dimensions of fuel compacts stored at ORNL

Name	Outer diameter (mm)			Inner diameter (mm)		Length (mm)	
	top	middle	bottom	top	bottom		
91OPB-1	26.05	26.06	26.07	10.00	10.01	39.01	38.99
	26.04	26.06	26.06			38.96	38.97
91OPB-13	26.05	26.05	26.05	10.01	10.02	39.01	38.99
	26.04	26.05	26.05			38.99	38.99
91OPB-14	26.04	26.05	26.06	10.01	10.01	38.97	38.98
	26.04	26.05	26.05			38.96	38.98
91OPB-18	26.04	26.05	26.06	10.00	10.01	39.02	39.01
	26.05	26.05	26.06			38.98	39.01
91OPB-23	26.04	26.06	26.06	10.00	10.01	39.01	39.00
	26.04	26.05	26.05			39.00	39.02
91OPB-24	26.05	26.05	26.05	10.01	10.02	39.03	39.00
	26.04	26.05	26.06			39.01	38.99
91OPB-25	26.04	26.05	26.05	10.02	10.02	39.03	39.04
	26.04	26.05	26.06			38.99	39.00
91OPB-26	26.05	26.06	26.06	10.01	10.02	39.07	39.03
	26.05	26.06	26.06			39.03	39.06

Table C.3 Dimensions of fuel compacts stored at JAERI

Name	Outer diameter (mm)			Inner diameter (mm)		Length (mm)	
	top	middle	bottom	top	bottom		
91OPB-4	26.04	26.05	26.05	10.01	10.02	38.99	38.97
	26.03	26.04	26.05			38.96	38.98
91OPB-5	26.03	26.04	26.05	10.02	10.02	39.01	39.02
	26.04	26.04	26.05			39.02	39.02
91OPB-6	26.03	26.04	26.06	10.01	10.02	38.99	38.96
	26.03	26.03	26.04			38.95	38.98
91OPB-16	26.04	26.04	26.04	10.00	10.01	39.01	38.97
	26.04	26.04	26.05			38.95	38.98
91OPB-19	26.02	26.04	26.05	10.01	10.02	39.03	39.03
	26.03	26.05	26.06			38.98	38.99
91OPB-20	26.03	26.04	26.05	10.02	10.02	39.02	38.98
	26.03	26.04	26.05			39.00	39.02
91OPB-27	26.03	26.04	26.06	10.01	10.02	39.01	39.00
	26.03	26.04	26.06			39.02	39.02
91OPB-28	26.04	26.04	26.04	10.01	10.02	39.00	39.00
	26.04	26.05	26.05			39.02	39.02
91OPB-29	26.04	26.04	26.04	10.01	10.01	38.97	38.96
	26.04	26.04	26.04			38.97	38.96
91OPB-30	26.03	26.04	26.05	10.01	10.02	39.01	39.03
	26.04	26.04	26.05			39.01	39.00

APPENDIX D CHARACTERISTICS OF FUEL COMPACTS

Table D.1 Characteristics of fuel compacts loaded in HRB-22 capsule

Name	Weight (g)	Density (Mg/m^3)	Packing fraction (%) Total	Fuel	Dummy	U content (g)
91OPB-2	34.292	1.94	33.9	6.8	27.1	2.283
91OPB-3	34.275	1.93	33.9	6.8	27.1	2.268
91OPB-7	34.287	1.94	33.9	6.8	27.1	2.323
91OPB-8	34.299	1.94	33.9	6.8	27.1	2.321
91OPB-9	34.286	1.94	33.9	6.8	27.1	2.311
91OPB-10	34.285	1.94	33.9	6.8	27.1	2.352
91OPB-11	34.298	1.94	33.9	6.8	27.1	2.316
91OPB-12	34.316	1.94	33.9	6.8	27.1	2.321
91OPB-15	34.282	1.94	33.9	6.8	27.1	2.318
91OPB-17	34.311	1.94	33.9	6.8	27.1	2.291
91OPB-21	34.274	1.93	33.9	6.8	27.1	2.349
91OPB-22	34.299	1.94	33.9	6.8	27.1	2.329

Table D.2 Characteristics of fuel compacts stored at ORNL

Name	Weight (g)	Density (Mg/m^3)	Packing fraction (%) Total	Fuel	Dummy	U content (g)
91OPB-1	34.274	1.93	33.9	6.8	27.1	2.260
91OPB-13	34.291	1.94	33.9	6.8	27.1	2.356
91OPB-14	34.310	1.94	33.9	6.8	27.2	2.354
91OPB-18	34.274	1.93	33.9	6.8	27.1	2.371
91OPB-23	34.244	1.93	33.9	6.8	27.1	2.348
91OPB-24	34.283	1.94	33.9	6.8	27.1	2.355
91OPB-25	34.258	1.93	33.9	6.8	27.1	2.356
91OPB-26	34.277	1.93	33.8	6.8	27.1	2.349

Table D.3 Characteristics of fuel compacts stored at JAERI

Name	Weight (g)	Density (Mg/m^3)	Packing fraction (%) Total	Fuel	Dummy	U content (g)
91OPB-4	34.307	1.94	33.9	6.8	27.2	2.268
91OPB-5	34.300	1.94	33.9	6.8	27.1	2.300
91OPB-6	34.327	1.94	34.0	6.8	27.2	2.289
91OPB-16	34.298	1.94	33.9	6.8	27.2	2.323
91OPB-19	34.275	1.94	33.9	6.8	27.1	2.328
91OPB-20	34.289	1.94	33.9	6.8	27.2	2.331
91OPB-27	34.281	1.94	33.9	6.8	27.1	2.306
91OPB-28	34.259	1.93	33.9	6.8	27.1	2.328
91OPB-29	34.257	1.94	34.0	6.8	27.2	2.302
91OPB-30	34.270	1.94	33.9	6.8	27.1	2.324